batteries

MDPI

*Review*

# Behavior of $NO_3^-$-Based Electrolyte Additive in Lithium Metal Batteries

**Jeongmin Kim [1], Taeho Yoon [2,*] and Oh B. Chae [1,*]**

[1] School of Chemical, Biological and Battery Engineering, Gachon University, Seongnam-si 13120, Republic of Korea
[2] Department of Chemical Engineering, Kyung Hee University, Yongin-si 17104, Republic of Korea
* Correspondence: tyoon@khu.ac.kr (T.Y.); obchae@gachon.ac.kr (O.B.C.)

**Abstract:** While lithium metal is highly desired as a next-generation battery material due to its theoretically highest capacity and lowest electrode potential, its practical application has been impeded by stability issues such as dendrite formation and short cycle life. Ongoing research aims to enhance the stability of lithium metal batteries for commercialization. Among the studies, research on N-based electrolyte additives, which can stabilize the solid electrolyte interface (SEI) layer and provide stability to the lithium metal surface, holds great promise. The $NO_3^-$ anion in the N-based electrolyte additive causes the SEI layer on the lithium metal surface to contain compounds such as $Li_3N$ and $Li_2O$, which not only facilitates the conduction of $Li^+$ ions in the SEI layer but also increases its mechanical strength. However, due to challenges with the solubility of N-based electrolyte additives in carbonate-based electrolytes, extensive research has been conducted on electrolytes based on ethers. Nonetheless, the low oxidative stability of ether-based electrolytes hinders their practical application. Hence, a strategy is needed to incorporate N-based electrolyte additives into carbonate-based electrolytes. In this review, we address the challenges of lithium metal batteries and propose practical approaches for the application and development of N-based electrolyte additives.

**Keywords:** lithium metal batteries; ether-based electrolytes; carbonate-based electrolytes; electrolyte additives; $LiNO_3$



**Citation:** Kim, J.; Yoon, T.; Chae, O.B. Behavior of $NO_3^-$-Based Electrolyte Additive in Lithium Metal Batteries. *Batteries* **2024**, *10*, 135. https://doi.org/10.3390/batteries10040135

Academic Editor: Seiji Kumagai

Received: 8 March 2024
Revised: 9 April 2024
Accepted: 11 April 2024
Published: 17 April 2024



## 1. Introduction

Current energy production, which relies on the combustion of fossil fuels, is expected to significantly impact ecosystems. Modern power storage technology, which involves electrochemical energy storage and conversion systems, is leaning towards the development of the battery industry to make these mechanisms more sustainable and eco-friendly [1,2]. Consequently, lithium-ion batteries have gained prominence, and research to improve their performance is ongoing [3–11]. The largest commercial application of lithium-ion batteries is in the small wearable battery industry, but demand for them is also growing in other industries, such as computers, cell phones, laptops, cameras, and electric vehicles [12]. Lithium-ion batteries offer advantages including low cost, long life, high specific energy and energy density, fast charge and discharge rates, and no memory effects [13–15]. The anodes of commercial lithium-ion batteries are mostly graphite or modified graphite, which has a rather low capacity per unit mass of 372 mAh $g^{-1}$ [16,17]. However, current lithium-ion batteries require advances in capacity and energy density per unit mass to fully penetrate into applications such as electric vehicle batteries. Carbon anodes, such as graphite, have been well researched and have nearly reached their theoretical capacity [18]. Further improvements in capacity and energy density are considered difficult [19]. Therefore, lithium metal is emerging as an anode material for next-generation batteries (Figure 1) [20,21].

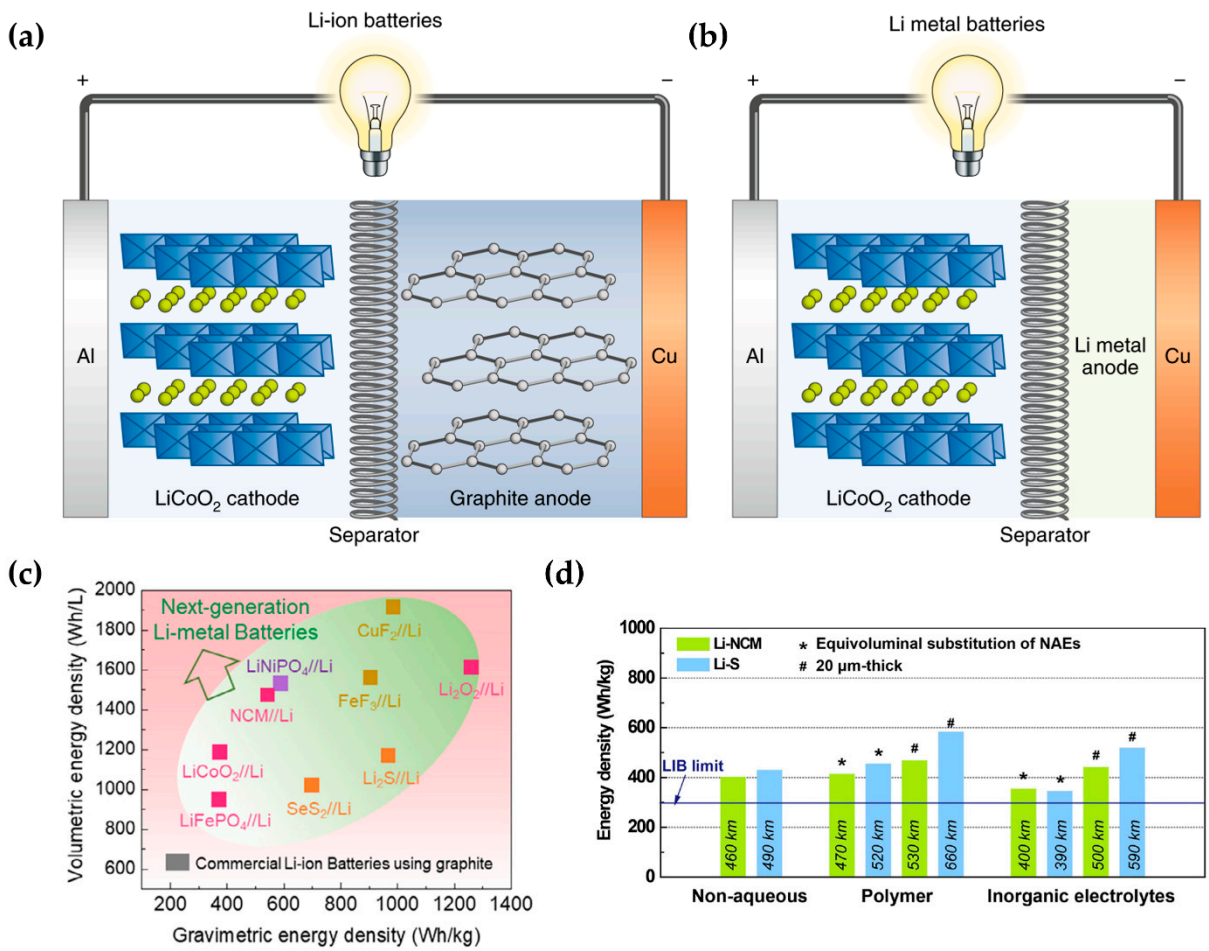


**Figure 1.** Importance of utilizing a lithium metal anode in lithium metal batteries. Schematic diagram of (**a**) graphite anode in Li-ion battery and (**b**) lithium metal battery [22]. Reprinted with permission from Ref. [22]. Copyright © 2019 nature. (**c**) Comparison table of energy densities of graphite anode and lithium metal anode [23]. Reprinted with permission from Ref. [23]. Copyright © 2020 ELSEVIER. (**d**) Current energy density limit of graphite cathode and expected energy density of battery with lithium metal anode [24]. Reprinted with permission from Ref. [24]. Copyright © 2020 ELSEVIER.

The theoretical capacity of lithium metal anodes is 3860 mAh $g^{-1}$, which is nearly 10 times that of graphite anodes. Additionally, they have the lowest reduction potential (−3.04 V vs. SHE) [22,24–26], allowing for a wide range of operating voltages. However, in lithium metal batteries, dendrites that grow on the surface of the metal anode cause low coulombic efficiency and short-circuiting of the cell [17,27,28]. In addition, owing to the large consumption of electrolytes and $Li^+$ ions during dendrite formation, lithium metal batteries have an inherently short lifetime [21,23]. Therefore, to improve performance, the key point is to improve the coulombic efficiency and stability of the battery. Many methods have been introduced to improve these: the addition of electrolyte additives to stabilize the solid electrolyte interface (SEI) layer [29,30], metal surface modification such as micro-patterning [31,32], introduction of artificial SEI layers such as polymer compresses or semiconductor thin films [33–39], doping of nanostructured materials to act as lithium hosts [40], and the development of solid electrolytes that can physically inhibit the growth of lithium metal dendrites [41–43]. Among these, the use of electrolyte additives is the simplest and most cost-effective strategy, and many studies have been conducted in this regard to improve the performance of lithium metal batteries. The use of N-based electrolyte additives, including $NO_3^-$ anions (hereafter referred to as N additives), which can incorporate $Li_3N$ and $LiN_xO_y$ into the SEI layer [44], has been studied

in ether-based and carbonate-based electrolytes. N additives can effectively inhibit the growth of lithium dendrites. However, the low solubility of N additives in carbonate-based electrolytes makes the direct use of N additives difficult [45]. In this review article, a systematic investigation of the effect of N additives in lithium metal batteries is presented, focusing on the effect of N additives on battery performance in ether-based electrolytes and their utilization in carbonate electrolytes. This will allow us to discuss directions for further and more effective improvements in the use of N additives in the current commercialized carbonate-based electrolytes.

## 2. Dendrite of Lithium Metal Batteries and Formation of Solid Electrolyte Interface

Lithium metal, lacking a $Li^+$ ion host, undergoes electrodeposition of $Li^+$ ions on its surface through plating/stripping during charging and discharging. This process results in severe volume changes in the lithium metal [46]. Additionally, $Li^+$ ions with high diffusion activation energy can form dendrites through local reduction on the surface of lithium metal, creating an aggregated structure with an inhomogeneous porous structure [47]. One of the advantages of lithium metal, its high reactivity owing to its low reduction potential, leads to rapid dendrite growth. As dendrites grow and separate into the electrolyte, dead lithium, which is not electrically conductive, accumulates in the cell, contributing to the degradation in capacity and stability of the cell [17,48,49]. Because these reactions occur at the interface between the lithium metal and the electrolyte, the interfacial reaction between them is important [50]. The lithium metal surface accumulates decomposition products from the reaction with the electrolyte, forming an SEI layer at the interface. This SEI layer prevents the physical contact between lithium metal and the electrolyte, inhibiting further corrosion [51]. The growth rate and growth behavior of lithium dendrites on the lithium metal surface depend on the strength, uniformity, thickness, and ionic conductivity of the SEI. An SEI layer generated in a pure lithium metal battery usually has a nonuniform surface (Figure 2a), partly due to different current densities, resulting in nonuniform electrodeposition of $Li^+$ ions [52,53]. With repeated charging and discharging, the changes in resistance and current density become more severe, and irreversible dendrite formation progresses (Figure 2b). As a result, the SEI layer has low mechanical strength and is easily destroyed through continuous charging and discharging [54]. The faster the battery charge rate and the higher the diffusion resistance of $Li^+$ ions in the SEI layer, the faster this phenomenon occurs. If the electrodeposition reaction rate of $Li^+$ ions is high, the $Li^+$ ions are depleted from the lithium metal surface, and the electrode reaction occurs in a diffusion-dominated manner, causing the interface to become unstable. To reduce the overpotential caused by this instability, the lithium metal anode interface requires a large surface area to increase the diffusion flux. For this reason and many others, vertically oriented dendrites are formed. As the dendrites grow, the SEI layer is destroyed, and another SEI layer is formed on the exposed lithium metal surface, which can lead to continuous electrolyte and lithium consumption.

Additionally, dendrites can cause issues such as increased metal surface area and side reactions, increased polarization, and decreased energy efficiency, contributing to the poor life characteristics of lithium metal batteries. Therefore, intense research is being conducted on electrolyte additives. Electrolyte additives can change the composition of the SEI layer simply and efficiently, which affects the output, lifetime, and temperature characteristics of the battery. In other words, electrolyte additives, especially those with $NO_3^-$, play a key role in stabilizing lithium metal batteries by creating a protective layer rich in inorganic materials, improving their performance [55]. In particular, N additives can generate favorable compounds, such as lithiophilic $Li_3N$, which plays a role in rapid ion conduction, and $LiN_xO_y$, which possesses high mechanical strength and high interfacial energy, in the SEI layer to increase the conductivity of $Li^+$ ions. Both compounds can effectively act as a passivation layer. Furthermore, high ion conductivity can induce uniform lithium nucleation on the surface of the lithium metal anode and effectively inhibit the formation of unstable lithium dendrites. Therefore, N compounds induce uniform

lithium nucleation on the surface of the lithium metal anode and effectively inhibit the formation of unstable dendrites physically and chemically [56].

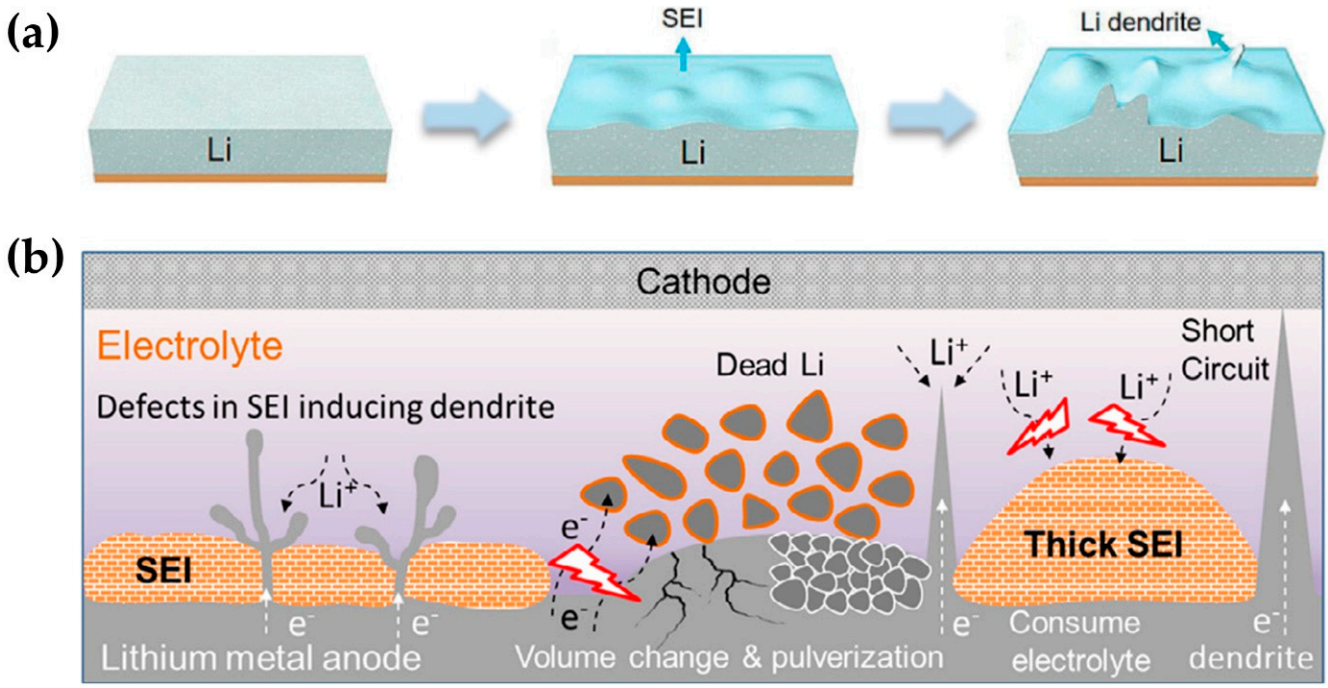


**Figure 2.** (**a**) Non-uniform electrodeposition and elution process of lithium metal anode and growth behavior of lithium dendrite [34]. Reprinted with permission from Ref. [34]. Copyright © 2017 WILEY–VCH. (**b**) The main causes of degradation of cell performance caused by dendrites [23]. Reprinted with permission from Ref. [23]. Copyright © 2020 ELSEVIER.

Moreover, N additives containing $NO_3^-$ demonstrate a notable electron-donating capacity towards $Li^+$ ions and function as potent oxidizers that swiftly interact with the lithium metal anode. Their donor number, measuring 22, surpasses those of commonly used electrolytes (EC, DMC [57], DME, DOL [58]). In electrolytes incorporating $NO_3^-$, the involvement of $NO_3^-$ in the solvation shell structure diminishes the presence of electrolyte molecules surrounding $Li^+$ ions. As a result, reducing the number of solvent molecules within the solvation shell can help mitigate the quantity consumed during the reduction process in the plating operation [57,59]. Furthermore, ensuring that the solvent remains unreduced requires a lowest unoccupied molecular orbital (LUMO) higher than that of the anode, which presents a challenging task to achieve. Nevertheless, $LiNO_3$ can serve as a promising alternative due to its lower LUMO compared to the solvent, enabling it to undertake the reduction role and mitigate solvent decomposition during SEI formation [60,61]. We could expect to improve the cycle stability of lithium metal batteries by using N additives.

## 3. $Li^+$ Ion Migration Mechanism of N Compounds in Solid Electrolyte Interfaces

As mentioned above, N additives change the composition of the SEI layer produced on the surface of the lithium metal anode in the electrolyte [62]. $LiNO_3$ salt, the most widely used N additive in SEI formation, reacts with the electrolyte components and lithium metal in the initial cycle and is converted into $LiNO_2$, $Li_3N$, and $Li_2O$, according to Equations (1) and (2). $Li_3N$ and $LiN_xO_y$ compounds are inorganic species, and the SEI layer containing them can improve mechanical strength and structural stability to inhibit lithium dendrite growth. In addition, this SEI layer has a high conductivity of $Li^+$ ions and can increase the diffusivity of $Li^+$ ions to induce the spherical electrodeposition of lithium and also the relatively uniform electrodeposition of $Li^+$ ions at high rates. $LiN_xO_y$ compounds are generally considered to be electrically stable, with low chemical activity and high ionic conductivity, which can

effectively protect the interface of lithium metal anodes. Moreover, a stable SEI layer can be formed even at a high temperature of 60 °C [63].

$$LiNO_3 + 2Li \rightarrow LiNO_2 + Li_2O \quad (1)$$

$$LiNO_2 + 6Li \rightarrow Li_3N + 2Li_2O \quad (2)$$

$Li_3N$ crystals are composed of $Li(2)_2N$ planes and a Li(1) plane that confines them [64–67]. As shown in Figure 3a, the Li(1) and $Li(2)_2N$ planes are separated. $Li^+$ ion migration is driven by intrinsic defects, an inherent property of $Li_3N$ crystals that allows $Li^+$ ions to move from occupied to unoccupied sites (defect-driven magnetism in bulk α-$Li_3N$) [68]. Intrinsic defects are represented by 'V' in Figure 3b. The anisotropy of conduction means that $Li^+$ ions seldom move along the c-axis (vertical) but predominantly along the a-axis and b-axis (in-plane). This can lead to the fast migration of $Li^+$ ions in the $Li_2N$ plane. Therefore, $Li_3N$ can dramatically improve $Li^+$ ion conductivity because of its high $Li^+$ ion mobility in the SEI layer and negligible electronic conductivity. Thus, it can play a key role as a shielding film at the interface of the lithium metal anode and electrolyte, while uniformly electrodepositing the lithium dendrite nuclei. Additionally, the N additive is reduced and decomposed before the lithium salt on the lithium metal anode surface, inducing the spherical deposition of lithium, which protects the solvent and lithium salt.

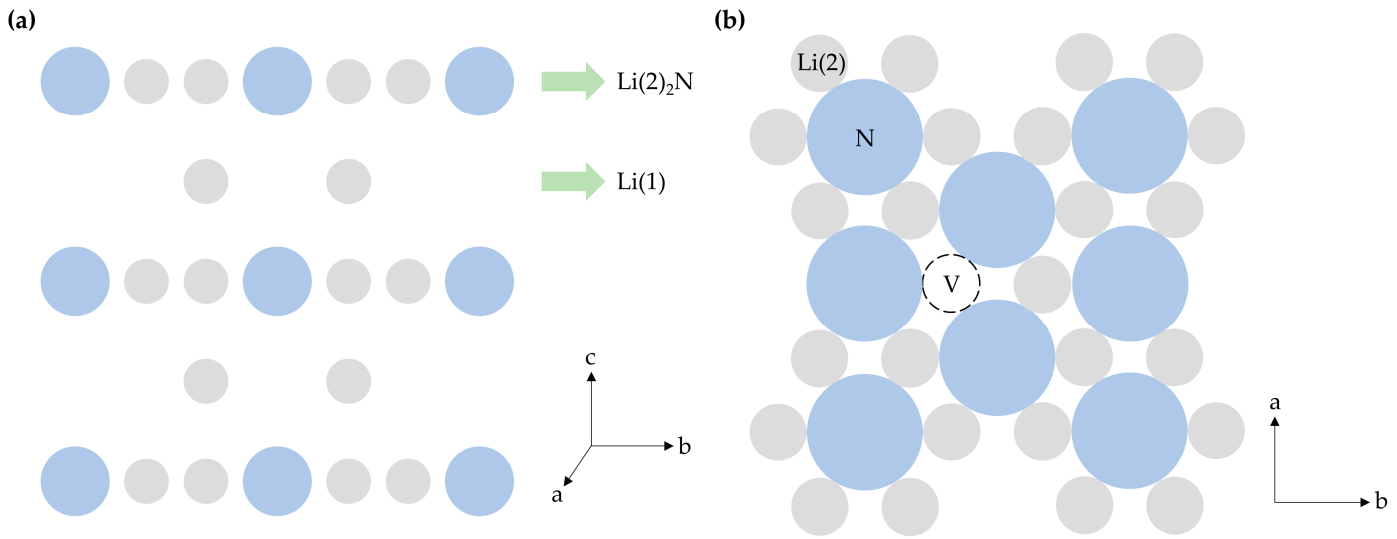


**Figure 3.** (**a**) Crystal structure of $Li_3N$ containing $Li(2)_2N$ plane and Li(1) plane and (**b**) cross-sectional view of $Li(2)_2N$ plane seen from above.

$Li_3N$ crystals are generally a mixture of α and β phases (Figure 4a,b). Generally, the α phase appears at room temperature about 25 °C, and the β phase appears at high pressure and high temperature [69,70]. Under room temperature conditions, the β phase can transition to the α phase, with no significant difference in ionic conductivity observed between the two phases. However, the activation energy for $Li^+$ ion diffusion is slightly different between the two phases. As shown in Figure 4c,d, the α phase is an amorphous crystal with a layered structure and the β phase is a structured crystal with a hexagonal structure, which is characterized by a difference in shape and ion conduction behavior. The β phase is stable at higher pressures than the α phase; therefore, it has been used in solid electrolytes. In α-$Li_3N$, Li ions move through Li(2) in the $Li_2N$ plane, but in β-$Li_3N$, Li ions move along a plane of pure Li(1). Figure 4c,d show the cluster model of α-$Li_3N$ and β-$Li_3N$ and the approximate distance of each element. The Li(2)–Li(2) distance of the α-$Li_3N$ crystal is shorter than the distances of Li(1(2))-N and Li(1)–Li(1). Similarly, the Li(1)–Li(1) distance of the β-$Li_3N$ crystal is shorter than the distances of Li(1(2))-N and Li(2)–Li(2). These results have implications for the migration of $Li^+$ ions because they

cause differences in the bond strengths between the elements. Ping et al. reported on the $Li^+$ ion removal energies and major charge carriers of α-$Li_3N$ and β-$Li_3N$ crystals [70]. Lithium removal energy is related to the bonding strength of the N atom to Li(2) and Li(1). α-$Li_3N$ and β-$Li_3N$ have the lowest $Li^+$ ion removal energies at 1.290 eV and 0.908 eV, respectively, and the farthest distances, at 2.107 Å and 2.326 Å from Li(2)-N and Li(1)-N, respectively. Therefore, the migration of $Li^+$ ions occurs in a direction perpendicular to the c-axis, and thus, they have good $Li^+$ ion conductivity. Additionally, a chemical treatment conducted by adding $H^+$ (proton) to α-$Li_3N$ crystals can weaken the Li(2)-N bonds in the $Li_2N$ plane, increasing the frequency of vacancies for $Li^+$ ions and thus resulting in better conductivity [66,71].

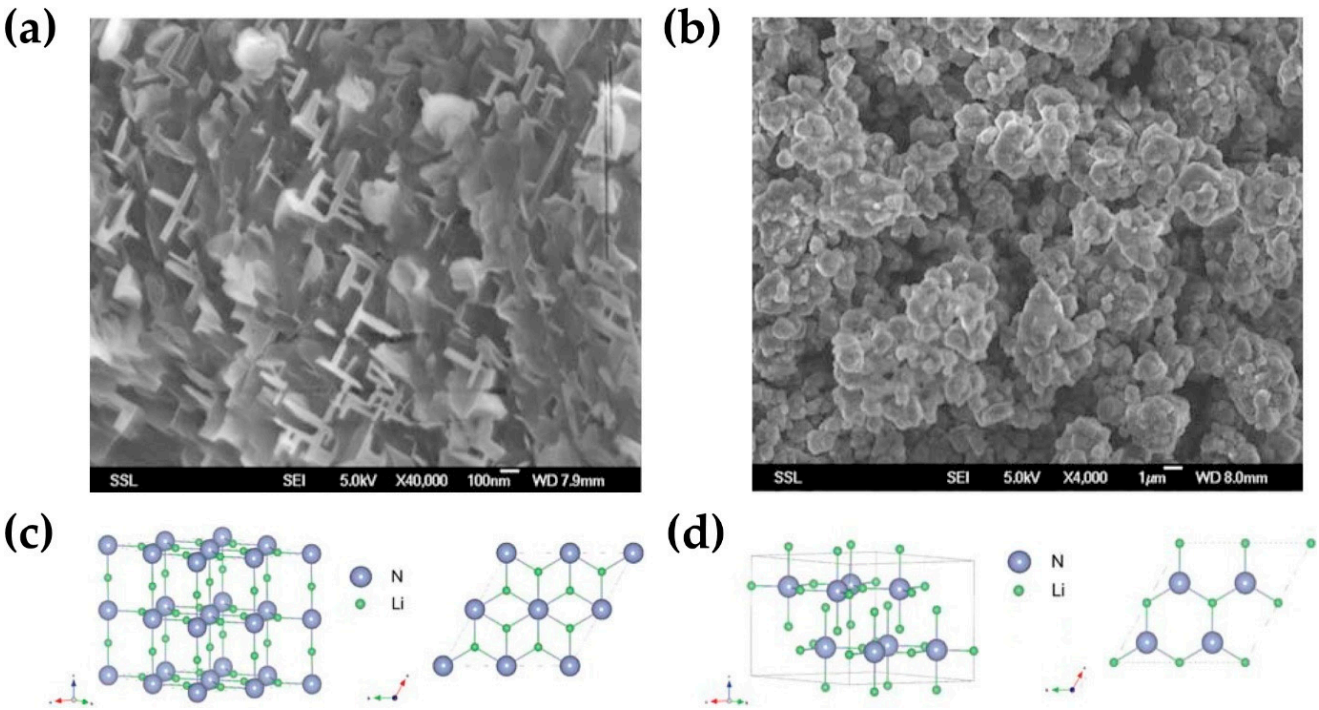


**Figure 4.** Scanning electron microscope (SEM) images of (**a**) α-$Li_3N$ crystal and (**b**) β-$Li_3N$ crystal. The cluster structure of (**c**) α-$Li_3N$ crystal and (**d**) β-$Li_3N$ crystal, viewed from directions perpendicular to and parallel to the c-axis, respectively [70]. Reprinted with permission from Ref. [70]. Copyright © 2010 Royal Society of Chemistry.

### *3.1. Ether-Based Electrolytes*

In ether-based electrolytes, $Li^+$ ions readily dissolve through strong coordination bonds with pairs of oxygen atoms, resulting in enhanced ionic conductivity that can boost cell performance. Additionally, given that the reduction stability of lithium metal in ether-based electrolytes is very high, stable electrodeposition and desorption reactions occur on the surface of the lithium metal anode, leading to a higher coulombic efficiency compared to carbonate-based electrolytes [52,72,73]. As previously discussed, the inclusion of N additives in lithium metal anodes effectively inhibits dendrite formation, thereby improving the overall lifespan performance of the cell. Figure 5 shows the effective dendrite inhibition of N additive in ether-based electrolyte.

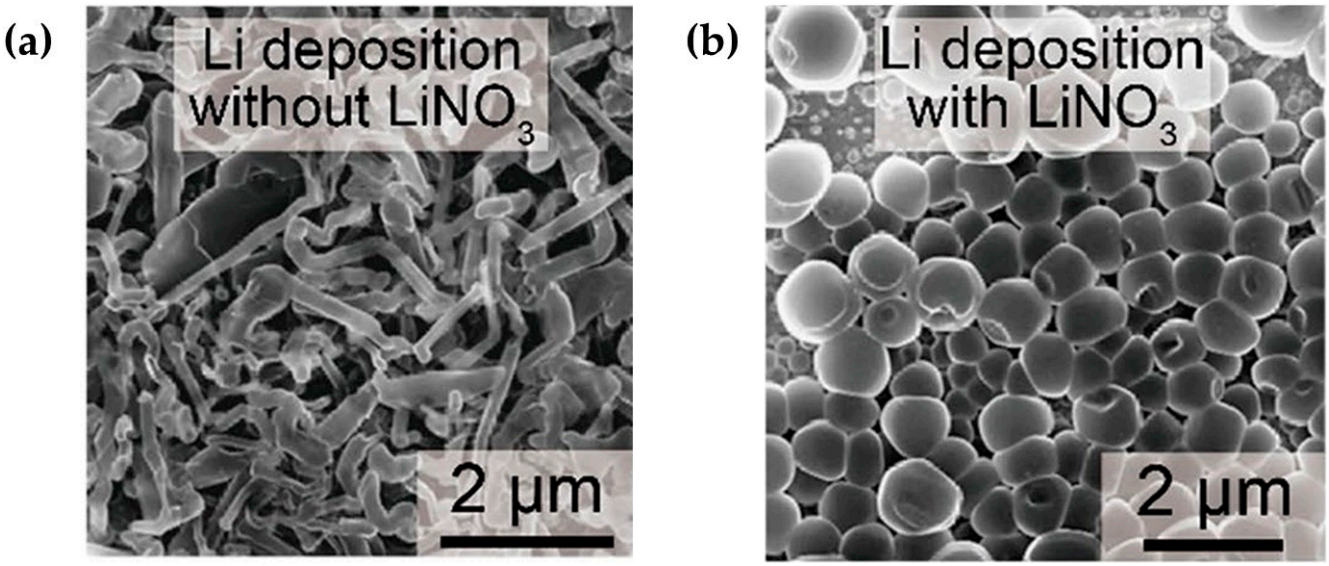


**Figure 5.** Scanning electron microscope (SEM) image of lithium dendrite on lithium metal anode using an ether-based electrolyte (**a**) without; (**b**) with $LiNO_3$ [46]. Reprinted with permission from Ref. [46]. Copyright © 2012 Springer Nature.

When incorporating $LiNO_3$ into an ether-based electrolyte, it is important to consider factors such as concentration [74] and gas generation [75]. These considerations are essential for optimizing the performance and safety of the electrolyte in various applications. Meanwhile, the solubility of $LiNO_3$ salt, which is commonly used as an N additive in ether-based electrolytes, is high, and it improves the mobility and transport rate of $Li^+$ ion as the salt concentration increases to up to 1 M, which is the soluble concentration of common lithium salts [76]. The conductivity of $Li^+$ ions is proportional to their concentration and mobility in the electrolyte, allowing them to dissolve easily. Therefore, N additives in ether-based electrolytes have been extensively studied. When the N additive is used as a single additive, dissolving large amounts, of 1 M or more, reduces the absolute "quantity" of the electrolyte solvent. As a result, this facilitates cooperation from anions in its dissolution structure, leading to stable cycling performance. However, this results in increased concentration, which adversely affects electrolyte wetting, and ion pairs begin to form, increasing the viscosity of the electrolyte and decreasing the ionic conductivity [77,78]. In contrast, studies have shown that by dissolving the N additive in a binary electrolyte or specific electrolyte, concentrations of 2 M or higher can be achieved without adversely affecting performance [79,80]. The dual additive strategy also allows for better synergy between the different efficacies of the N additive and the other salts, as well as their different potencies.

Figure 6 shows the solubility and cycling performance of the cells with 1 M $LiNO_3$, 4 M LiFSI, and salts of both 2 M $LiNO_3$ and 2 M LiFSI. A quantity of 2 M of $LiNO_3$ has a positive binding energy and is insoluble in the electrolyte (Figure 6a). However, when combined with LiFSI salt, (Figure 6b), it can be intuitively seen that it is soluble up to 2 M. Commercial cathodes (NCM and LFP) were used to evaluate the performance of the electrolytes. The capacity and coulombic efficiency of the cells show an overall increase with LiFSI, which forms a LiF-based SEI layer to improve the cycling stability and reversibility of lithium in lithium metal batteries [81], and $LiNO_3$, which induces a spherical deposition morphology of lithium (Figure 6f–i), and the interfacial resistance between the lithium metal anode and electrolyte drops (Figure 6c).

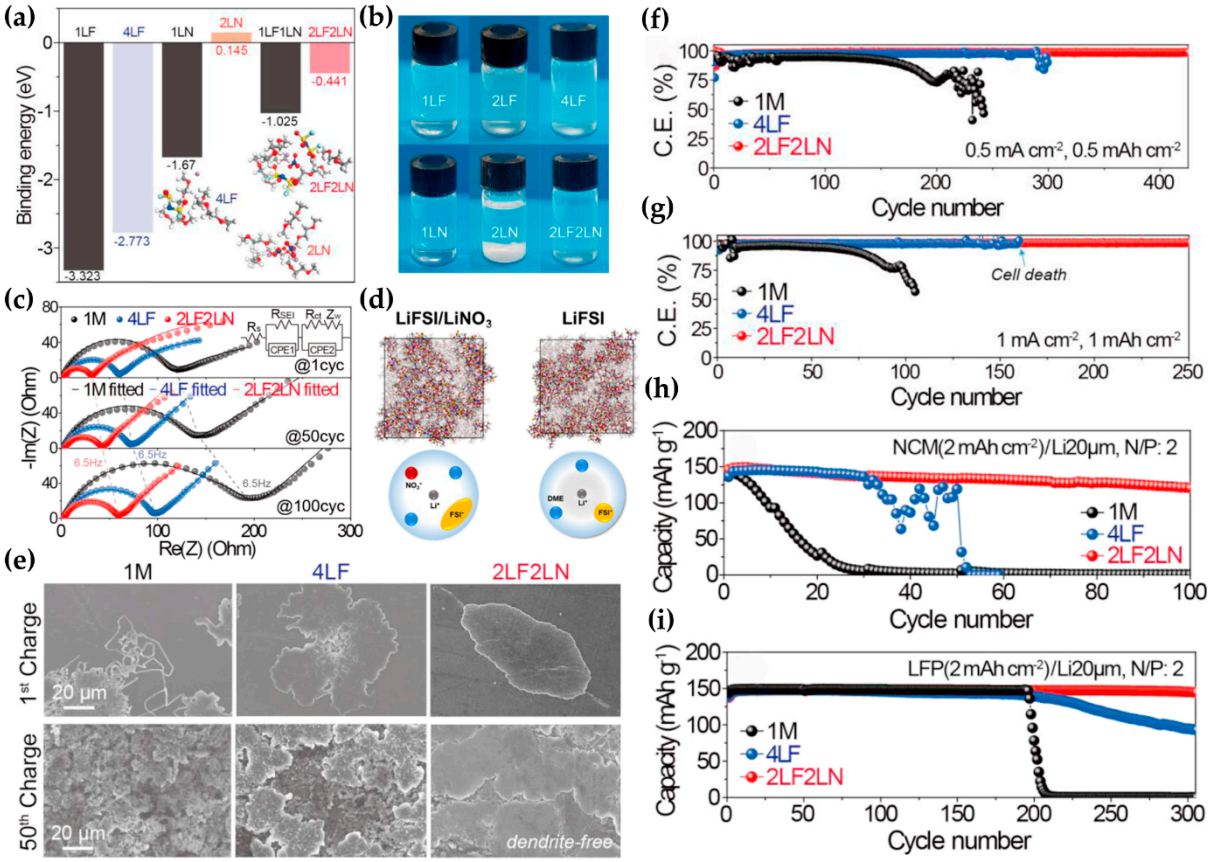


**Figure 6.** (**a**,**b**) Photographs showing solubility of $LiNO_3$ and $LiPF_6$ in ether-based electrolyte. (**f**–**i**) Improvements in capacity and coulombic efficiency with and without the N additive in ether-based electrolyte environment. (**c**) Electrochemical impedance spectroscopy (EIS) spectra of 2LF2LN in 1,2-dimethoxyethane (DME) electrolyte [82]. Reprinted with permission from Ref. [82]. Copyright © 2021 ELSEVIER. (**d**) Schematic diagram of $Li^+$ ion dissolution sheath structure of LiFSI [81]. Reprinted with permission from Ref. [81]. Copyright © 2019 American Chemical Society. (**e**) Scanning electron microscope (SEM) images of lithium metal surface with electrolytes added with 1 M $LiNO_3$, 4 M LiFSI, and both 2 M $LiNO_3$ and 2 M LiFSI. Cycling performance of dual salt added electrolyte. coulombic efficiency of Li||Cu asymmetric cells using electrolytes added with 1 M $LiNO_3$, 4 M LiFSI, and both 2 M $LiNO_3$ and 2 M LiFSI after the 1st and 50th Li platings at (**f**) 0.5 mA $cm^{-2}$ and 0.5 mAh $cm^{-2}$ and (**g**) 1 mA $cm^{-2}$ and 1 mAh $cm^{-2}$. The discharge capacity of (**h**) Li||NCM811 cell and (**i**) Li||LFP cell [82]. Reprinted with permission from Ref. [82]. Copyright © 2021 Elsevier.

Figure 6f shows the coulombic efficiency under the test conditions of 0.5 mA $cm^{-2}$ and 0.5 mAh $cm^{-2}$ for an asymmetric cell with copper foil as the reaction electrode and lithium metal as the reference electrode. Figure 6g shows the coulombic efficiency under the test conditions of 1 mA $cm^{-2}$ and 1 mAh $cm^{-2}$ for an asymmetric cell with copper foil as the reaction electrode and lithium metal as the reference electrode. Unlike the 1 M $LiNO_3$-added and 4LF-added electrolytes, which show cycle fading before 300 and 150 cycles, respectively, the cell with 2 M $LiNO_3$ and 2 M LiFSI shows an average coulombic efficiency of 98.5% after more than 420 and 250 cycles. Figure 6h,i show the capacity performance of the cells using commercial cathodes, NCM (areal capacity of cathode: 2 mAh $cm^{-2}$) and LFP (areal capacity of cathode: 2 mAh $cm^{-2}$), respectively, which also show a performance improvement. Figure 6e shows that the lithium metal anode surface in each cell becomes uniform and stable. These two additives are used together to solve the problem of the low solubility of $LiNO_3$ and its depletion due to continuous consumption. LiFSI inhibits the aggregation of $LiNO_3$ in 1,2–dimethoxyethane (DME), allowing it to maintain its efficacy for a longer period and dissolve up to 2 M. (Similar results can be seen with the

addition of LiTFSI salts). This procedure has been described previously. Figure 6d shows a schematic illustrating how $FSI^-$ dissociates $LiNO_3$ molecules. This dual salt electrolyte is also characterized by a broader oxidation window owing to the reduction of the electrolyte due to the high concentration effect, allowing for the use of a high-voltage cathode [82]. This result is consistent with the result for cells with 1 M $LiNO_3$ and LiFSI added [83].

Figure 7 shows the synergistic effect of polysulfide and N additive dual salts in an ether-based electrolyte. Adding only $LiNO_3$ to the cells leads to improved performance; however, when $LiNO_3$ is added to the electrolyte as a dual salt with polysulfide, the performance is dramatically improved [79,84,85]. The addition of polysulfide to $LiNO_3$ makes the lithium metal surface significantly cleaner, as shown in Figure 7a. In Figure 7b,c,e,f, both EIS spectra and voltage profiles with and without $LiNO_3$ addition show the stability of the modified SEI. It can be seen that by adding both, the internal resistance decreases. Figure 7d,g show schematic diagrams of the stable evolution of the SEI layer when polysulfide and $LiNO_3$ are used together in an ether-based electrolyte. Studies have shown that adding these two salts to diethylene glycol dimethyl ether, diglyme (G2 solvent) improves the performance through high solubility [79].

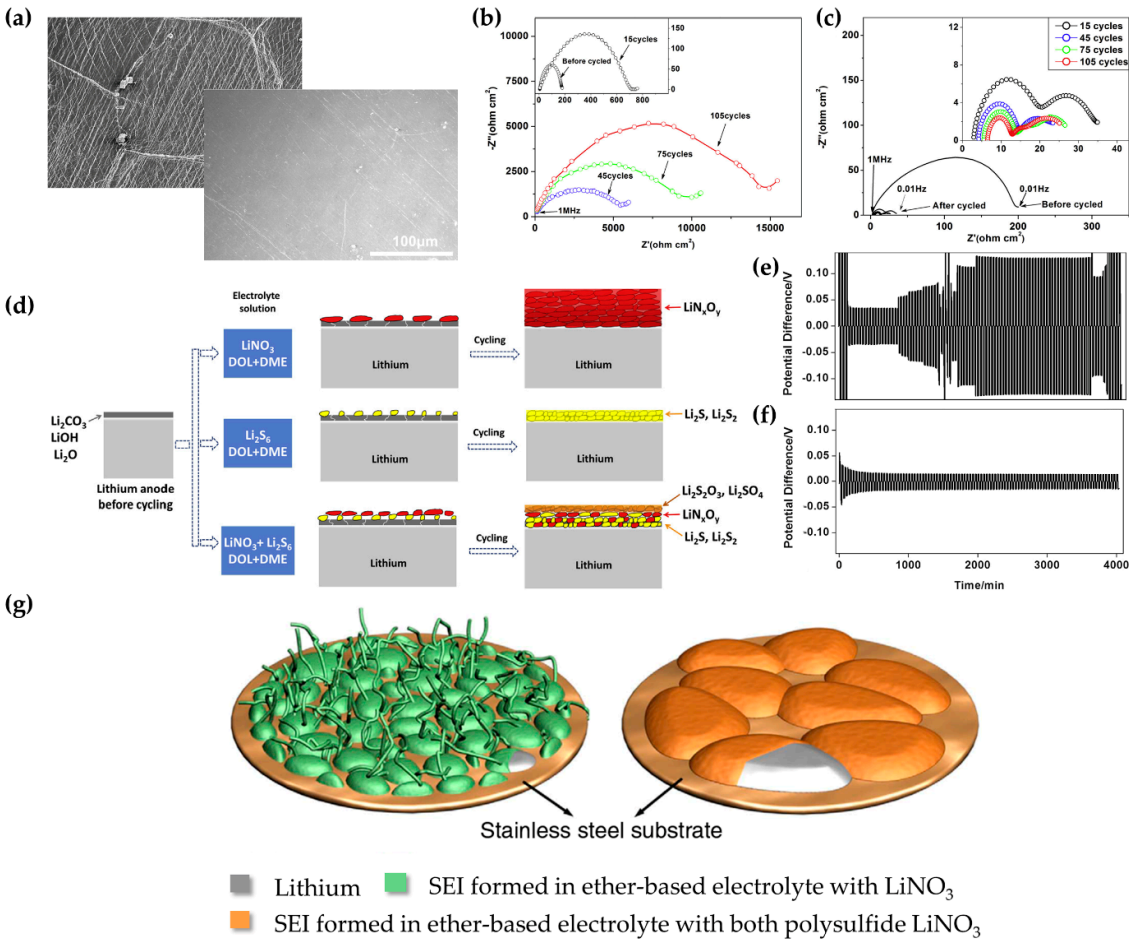


**Figure 7.** Performance of cells adapted to ether-based electrolyte with polysulfides and N additive. (**a**) Scanning electron microscope (SEM) image of lithium metal surface in dioxolane (DIOX)/dimethoxyethane (DME) electrolyte. Electrochemical impedance spectroscopy (EIS) spectra of Li||Li cells with (**b**) $LiNO_3$ only and (**c**) polysulfide and $LiNO_3$. (**d**) Schematic diagram of better SEI layer generation. Voltage profile of Li||Li cells in electrolyte with (**e**) $LiNO_3$ only and (**f**) both polysulfide and $LiNO_3$ [85]. Reprinted with permission from Ref. [85]. Copyright © 2014 ELSEVIER. (**g**) Model of electrodeposition of ether-based electrolyte with polysulfide and $LiNO_3$ on the lithium metal surface of the applied cell [84]. Reprinted with permission from Ref. [84]. Copyright © 2015 nature.

In addition, there are cases of batteries that can retain the performance of the cell for a longer period by adopting the method of combining N additives with the self-healing electric shield (SHES) mechanism, which shows electrostatic shielding behavior (Figure 8a) [86–88]. Not only does the addition of $CsNO_3$ [89], $RbNO_3$ [90], and $KNO_3$ salts [91] stabilize the surface of the lithium metal anode due to the generation of N compounds, but spherical lithium deposition and low resistance were observed due to $K^+$ ions causing electrostatic shielding phenomena. This shows the possibility of increasing the coulombic efficiency of lithium metal cells and even increasing their capacity, fast charge, and discharge. The SHES mechanism is effective in preventing dendrites by reducing the concentrations of $Cs^+$, $Rb^+$, and $K^+$, which inherently have a higher reduction potential than $Li^+$, and thus their reduction potential will be lower than that of $Li^+$. This mechanism consumes very few metal cations. The reduction potential of the metal cations is strongly related to their concentration, which follows the Nernst equation (Equation (3)).

$$E_{Red} = E^{\varnothing}_{Red} - \frac{RT}{zF} \ln \frac{\alpha_{Red}}{\alpha_{Ox}} \tag{3}$$

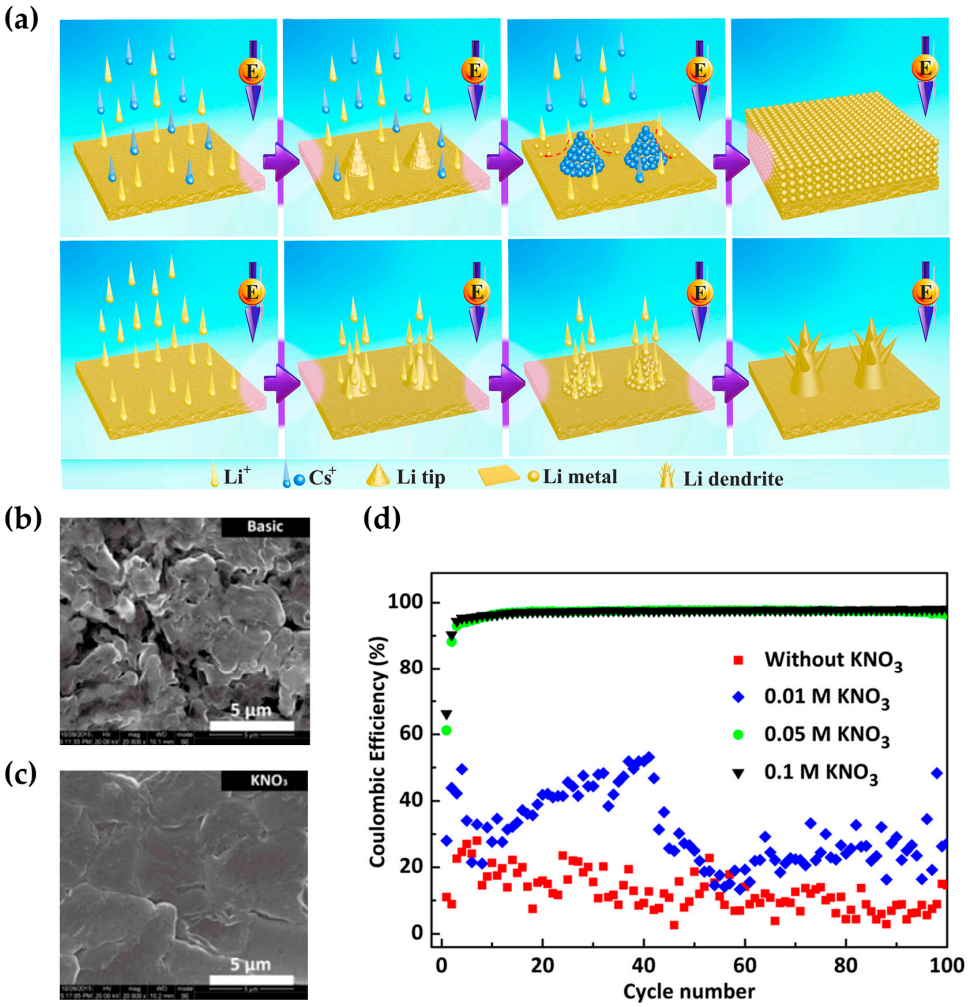


**Figure 8.** (**a**) N additive combined with the self-healing electric shield (SHES) mechanism. (**a**) Schematic illustration of the SHES mechanism [86]. Reprinted with permission from Ref. [86]. Copyright © 2019 ELSEVIER. Scanning electron microscope (SEM) images of lithium metal surface using ether electrolyte (**b**) without $KNO_3$ and (**c**) with $KNO_3$. (**d**) Coulombic efficiency of Li–Cu cells for different concentrations of $KNO_3$ added in 1 M LiTFSI in 1,2-dimethoxyethane (DME)/1,3-dioxolane (DOL) electrolyte [91]. Reprinted with permission from Ref. [91]. Copyright © 2016 PubMed.

Electrolytes containing $K^+$, which is another shielding cation, have also been widely studied for $Li^+$ plating/stripping stability [92,93]. Figure 8b,c show the SEM images with and without $KNO_3$ added. It can be seen that $KNO_3$ played a good role as a N additive, resulting in high-density and stable lithium electrodeposition. Figure 8d shows the coulombic efficiency of an asymmetric cell when $KNO_3$ is added to an ether-based electrolyte. Compared with the bare electrolyte, the cell with 0.05–0.1 M of $KNO_3$ shows much improved performance.

### *3.2. Carbonate-Based Electrolytes*

Carbonate-based electrolytes, which are widely used in commercial $Li^+$ ion batteries, reductively degrade at voltages between 1.5 V and 0.6 V (vs. $Li/Li^+$) to form an SEI layer on the anode surface [94]. Because of their low oxidation stability, ether-based electrolytes with a typical 1 M lithium salt undergo violent degradation in high-voltage (>4 V) batteries. In comparison, carbonate-based electrolytes have excellent oxidation stability at high voltages [95,96]. Therefore, to add N additives in electrolyte of commercialized high-voltage batteries, the ether solvent must be converted into an ester solvent with high oxidation stability [97]. However, N additives are almost insoluble in carbonate-based electrolytes, which are organic solvents (approximately 0.012 M [98]) [45]. Several strategies have been developed to address this problem. If the solubility issues are resolved, N additives can run normally in carbonate-based electrolytes, and a stable SEI layer is formed. In carbonate-based electrolytes, the N additive first reacts with the lithium metal anode to form an SEI layer owing to its reduction potential being higher than that of the electrolyte components (Figure 9a). Nowadays, through some processing, researchers are able to dissolve the N additives in a carbonate-based electrolyte to create an SEI layer containing the N compound. The SEI layer creates an appropriate pressure on the lithium metal surface and facilitates the movement of $Li^+$ ions, resulting in the formation of a highly uniform spherical dendrite compared to the bare electrolyte (Figure 9b,c). Therefore, in the following part of this section, we will focus on the solubility of N additives in carbonate-based electrolytes.

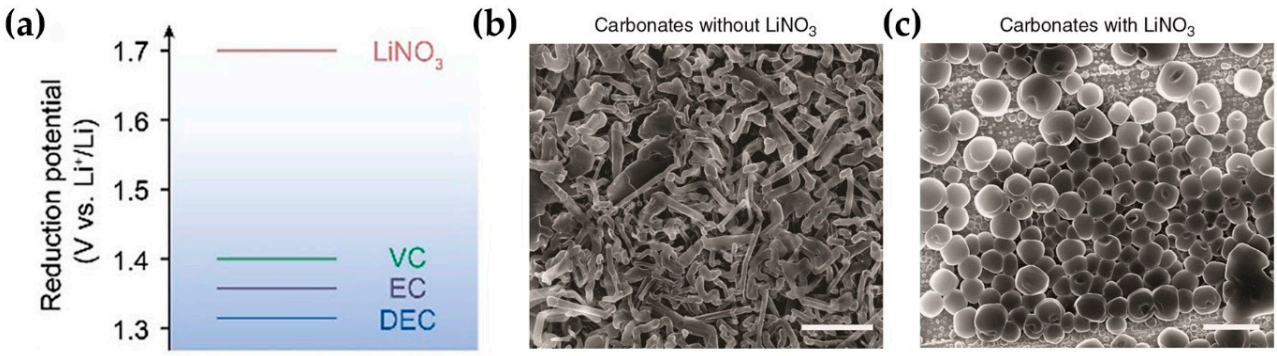


**Figure 9.** (**a**) Reduction potential table of representative carbonate-based electrolyte materials [46]. Reprinted with permission from Ref. [46]. Copyright © 2012 SPRINGER NATURE. Scanning electron microscope (SEM) images showing the effect of $LiNO_3$ in carbonate-based electrolytes: (**b**) bare (**c**) addition of $LiNO_3$ to simple ethylene carbonate (EC)/diethyl carbonate (DEC) [98]. Reprinted with permission from Ref. [98]. Copyright © 2018 nature.

In general, strategies to aid the dissolution of N additives include introducing other additives that can increase the solubility or using a binary electrolyte. The most popular method used to improve the solubility of the N additive is to dissolve $LiNO_3$ in a carbonate-based electrolyte using the solubilizing agent $CuF_2$. Trace amounts of $CuF_2$ salts act as a catalyst to promote the dissolution of $LiNO_3$ without participating in the reaction within the cell. Previous studies have suggested that the effect of $CuF_2$ is based on the fact that compared to $Li^+$ ions, $Cu^{2+}$ ions exhibit a stronger affinity for $NO_3^-$, and that $Cu^{2+}$-$NO_3^-$ complexes are formed in the EC/DMC electrolyte [99]. Figure 10b–e show the capacity performance and EIS spectra of cells with LFP (areal capacity of cathode: 1.0 mAh $cm^{-2}$)

and NCA (areal capacity of cathode: 2.5 mAh $cm^{-2}$) cathodes for lithium metal batteries containing CuF + $LiNO_3$ in 1 M $LiPF_6$ in EC/DEC (1:1 $v/v$), respectively. Additionally, it has been reported that the addition of CsF salts to conventional carbonate-based electrolytes increases the solubility of $LiNO_3$ [100]. Because the $Cs^+$ ions in CsF salts have a minimum charge compared to the metal ion radius, the solubility of $LiNO_3$ can be increased through cation size effects that lower the localization density of the charge. When the salts are added together, few solvent-degraded molecules are found in the SEI layer and inorganic molecules with relatively high mechanical strength are found. This can lead to significant improvements in the capacity performance and ion migration resistance of lithium metal batteries (Figure 10f–j). It has been reported that $Sn^{4+}$ [101], $Al^{3+}$, and $In^{3+}$ [102] ions have similar effects. The inhomogeneous electrodeposition of $Li^+$ ions is also inhibited by the presence of $Cs^+$ ions, which exhibit an electrostatic shielding effect. The N 1s XPS spectra show the composition of the SEI layer generated in the electrolyte and on the electrode surface. The N 1s XPS spectra show that the N additive is well dissolved in the EC/DEC electrolyte, and $Li_3N$ and $LiN_xO_y$ are generated in the SEI by the N additive at the electrode interface (Figure 10a,f). Figure 10k shows that the solubility of $LiNO_3$ with CsF is improved. Solubilizers that use a similar mechanism to improve the solubility of N additives include $BF_3$ [103,104], tris(pentafluorophenyl)borane (TPFPB) [105], and tin(II) [106].

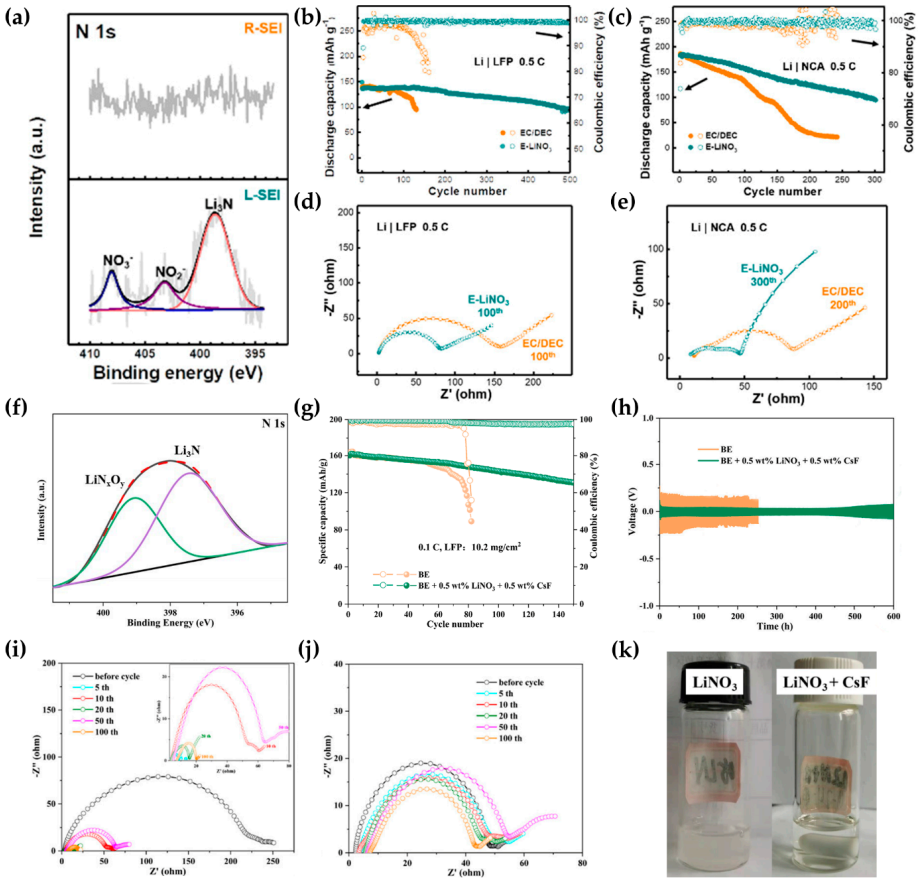


**Figure 10.** Performance of cells with solubilizers (salts) of N additive. (**a**,**f**) N 1s X-ray photoelectron spectroscopy (XPS) spectra in ethylene carbonate (EC)/diethyl carbonate (DEC) electrolyte without/with the N additive. (**b**–**e**) Performance of Li||LFP and Li||NCA cells using 1 M $LiPF_6$ dissolved in EC/DEC (1:1 $v/v$) with trace amounts of CuF and 1.0 wt% $LiNO_3$ [99]. Reprinted with permission from Ref. [99]. Copyright © 2018 WILEY-VCH. (**g**–**j**) Performance of Li||LFP cell using 1 M $LiPF_6$ in EC/DEC (1:1 $v/v$) dissolved with 0.5 wt% CsF and 0.5 wt% $LiNO_3$. (**k**) Visible solubility difference between electrolytes with dissolved pure $LiNO_3$ and both CsF and $LiNO_3$ in EC/DEC electrolyte [100]. Reprinted with permission from Ref. [100]. Copyright © 2023 Royal Society of Chemistry.

In addition, there are some strategies using a binary electrolyte that facilitate the dissolution of $LiNO_3$. Pyridine has a high donor number (DN), which is a measure of the ability of the solvent to solubilize cations and Lewis acids, and has been shown to dissolve up to 4.5 M $LiNO_3$. By adding a small amount of saturated $LiNO_3$-pyridine solvent to 1 M $LiPF_6$/EC-ethyl methyl carbonate (EMC)-DMC (1:1:1 vol%), the effect of adding $LiNO_3$ lithium salt to a carbonate-based electrolyte can be achieved [107]. Figure 11a,c,d,f show that the N additive dissolved in pyridine solvent dissolves well in the carbonate-based electrolyte. The N additive dissolved in the pyridine solvent dissolves in a carbonate-based electrolyte while reducing the overvoltage and ion migration resistance of the cell (Figure 11b,e). Tetraethylene glycol dimethyl ether (TEGDME) [108,109] with a wide potential window can improve cycling performance through the influence of $LiNO_3$ salts. Figure 11l shows a schematic illustration of the activity of TEGDME in an electrolyte. TEGDME can change the solvation structure of $Li^+$ ions in the electrolyte, which promotes the dissolution of the N additive in the carbonate-based electrolyte. Thus, TEGDME can reduce the overvoltage and $Li^+$ ion migration resistance of the cell (Figure 11g,h,i). Figure 11j,k show enhanced cycling performance resulting from the activation of TEGDME. In addition, additives using solvents such as EC/LiDFOB electrolytes with a small amount of TEP/$LiNO_3$ solvent to improve the solubility of N additives in carbonate-based electrolytes are widely known [110]. Additionally, gamma–butyrolactone (GBL) solvent has a high DN, which leads to the high solubility of $LiNO_3$, and studies are being conducted in this regard to dissolve $LiNO_3$ and add it to carbonate-based electrolytes to confirm the effectiveness of N additives in carbonate-based electrolytes [111].

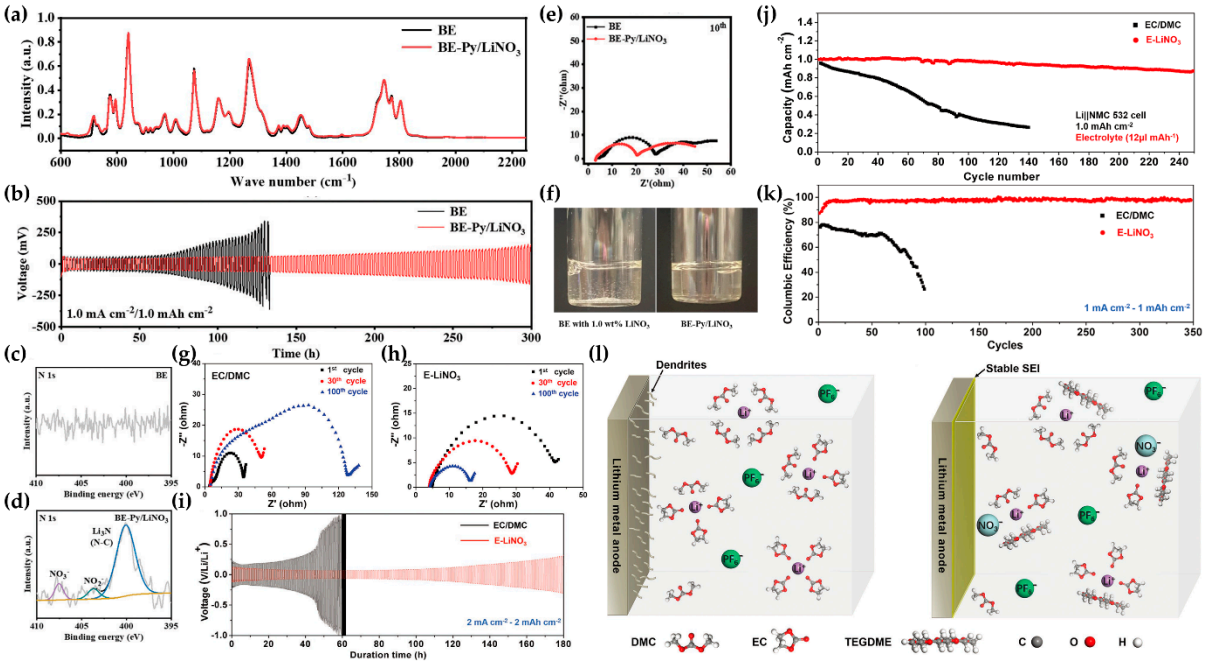


**Figure 11.** Performance of cells with solubilizers (solvents) of N additive. (**a**–**e**) Performance of cells with pyridine solvent dissolved $LiNO_3$ in carbonate-based electrolyte: (**a**) Fourier transform infrared spectroscopy (FTIR); (**b**) voltage profile, N 1s X-ray photoelectron spectroscopy (XPS) spectra (**c**) without and (**d**) with pyridine solvent including N additives, and (**e**) electrochemical impedance spectroscopy (EIS) spectra. (**f**) The picture of bottles for checking solubility [107]. Reprinted with permission from Ref. [107]. Copyright © 2021 Royal Society of Chemistry. (**g**–**k**) Performance of cells with tetraethylene glycol dimethyl ether (TEGDME) solvent dissolved $LiNO_3$ in carbonate-based electrolyte: EIS spectra (**g**) without and (**h**) with TEGDME solvent including N additive, (**i**) voltage profile and (**j**,**k**) cycle performance. (**l**) Schematic representation of the solvation structure of an electrolyte [108]. Reprinted with permission from Ref. [108]. Copyright © 2020 PubMed.

In the above discussion, a strategy of using additives focusing solely on solubility was introduced. However, this method does not have a significant effect on the performance of the cell because it involves injecting salt into the electrolyte, which has no effect on performance. Therefore, research has been conducted to identify additives that can have a positive effect on performance. This section covers dual salts and binary electrolytes, which have a synergistic effect that can simultaneously improve performance while increasing solubility. In a 1.0 M $LiPF_6$ in 1:1 $v/v$ ethylene carbonate (EC)/diethyl carbonate (DEC) electrolyte saturated with $LiNO_3$ dual salt electrolyte, the two salts increase the stability of the lithium metal cathode through a competitive dissolution mechanism. In this electrolyte, the $NO_3^-$ anion changes the dissolution structure by relaxing the interaction between the solvent molecules and $Li^+$ ions, and the preferential reduction of $NO_3^-$ promotes the formation of a mineral-rich SEI film and prevents the preferential degradation of the $LiPF_6$ salt, which can be continuously utilized for charging and discharging [98]; 1.0 M $LiPF_6$ and 1.1 wt% $LiNO_3$ dissolved in fluoroethylene carbonate (FEC)/DMC/DME (3.5:3.5:3 vol%) (FEC/$LiNO_3$ electrolyte) shows a significant increase in the capacity performance and coulombic efficiency of the cell (Figure 12a), and a significant decrease in the interfacial resistance growth trend compared to the conventional 1.0 M $LiPF_6$ EC/DEC-using cell (Figure 12b) [112]. $LiNO_3$ is not the only N additive, and other N additives can indeed be used with equal efficacy. In a cell with 0.05 M $Y(NO_3)_3$ and 5 vt% FEC added into 1 M $LiPF_6$ in EC/DMC (1:1 vol), molecular dynamics simulations show that due to the unfixed coordination number of rare earth cations, the Y cation changes the solvation structure of $Li^+$ ions in the electrolyte. Consequently, it has better solubility than $LiNO_3$ in carbonate-based electrolytes [113]. When combined with fluoroethylene carbonate (FEC) in the same electrolyte, the interstitial groups generated by the electrochemical reaction favor dense lithium deposition. Consequently, stable and high coulombic efficiencies are achieved for Li/Cu cells in commercial carbonate electrolytes using these additives (Figure 12c). Li/Li symmetric cells can be operated for more than 1000 h at a current density of 1 mA $cm^{-2}$. In addition, the NCM811/Li full cell exhibits excellent cycling stability and improved rate performance [113]. The solubility-increasing effect of FEC is also observed in the interaction with KNO3 [93].

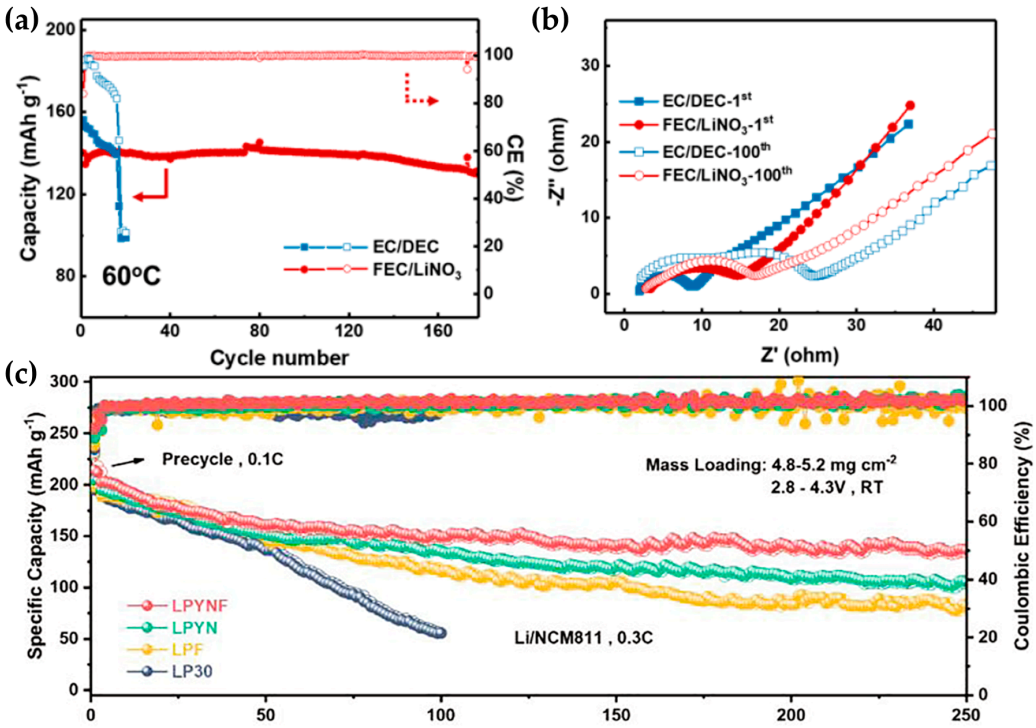


**Figure 12.** *Cont.*

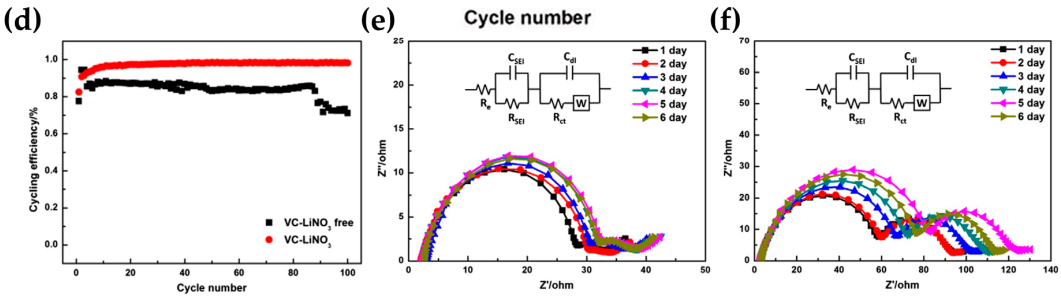


**Figure 12.** Cycling performance of cells with (**a**) FEC/LiBOB with $LiNO_3$ [112], (**c**) FEC with $YNO_3$ [113], (**d**) 1 M $LiPF_6$ in EC/DEC electrolyte and added $LiNO_3$-VC additive [114]. Reprinted with permission from Ref. [112]. Copyright © 2018 Wiley–VCH. Reprinted with permission from Ref. [113]. Copyright © 2022 ELSEVIER. Reprinted with permission from Ref. [114]. Copyright © 2015 Elsevier. EIS spectra of cells with (**b**) FEC/LiBOB with $LiNO_3$ [112], (**e**,**f**) 1 M $LiPF_6$ in EC/DEC electrolyte and added $LiNO_3$-VC additive [114]. Reprinted with permission from Ref. [112]. Copyright © 2018 Wiley–VCH. Reprinted with permission from Ref. [114]. Copyright © 2015 Elsevier.

Here is a similar example of improving cell performance by adding a solvent and salt together with the N additive. As mentioned earlier, changing the solubility structure of the N additive is the most widely used method for increasing the solubility of the N additive in carbonate-based electrolytes. In the cell that immediately follows, $RbPF_6$, $LiNO_3$, and 18-crown-6 are added together to an FEC/EC/DEC electrolyte [115]. The low LUMO and high highest occupied molecular orbital (HOMO) of 18-crown-6 in 18-crown-6-$Rb^+$ electrolytes, based on the shielding layer effect surrounding the nucleus, can prevent $Li^+$ from being deposited on the lithium dendrites by the resulting Rb(18-crown-6)$^+$ complexes while preventing the reduction of $Rb^+$ to lithium metal in conventional electrolytes. Moreover, the coordination of Rb(18-crown-6)$^+$ can promote the solubility of the N additive in the carbonate-based electrolytes. The cell exhibits a high coulombic efficiency owing to the high stability caused by the SHES effect, in addition to the N additive effect, indicating the possibility for practical use. Additionally, vinylene carbonate additives have been reported to exhibit good performance when dissolved in carbonate-based electrolytes with $LiNO_3$. Figure 12d–f show that the $LiNO_3$-VC dual additive exhibits improved performance in terms of coulombic efficiency and ion transfer resistance [114]. In addition, a study showing the synergy effect of LiFSI, $LiPF_6$ and $LiNO_3$ in a carbonate-based electrolyte has been reported [116].

The above method has been adopted as an excellent strategy for utilizing the efficacy of N additives; however, only a relatively small quantity of $LiNO_3$ can be dissolved in the electrolyte, leading to the rapid depletion of $LiNO_3$ with self-sacrificial properties. Although the method has been shown to effectively inhibit dendritic cells and significantly improve cycling performance, the high cycling performance of lithium metal batteries cannot be maintained for a long time. Therefore, another approach has been developed to overcome the high solubility barrier of carbonate-based electrolytes. Researchers use cells containing $LiNO_3$ nanoparticles encapsulated in porous polymeric gels [98,117]. This can provide 10 times more N than the direct dissolution of a typical N additive, allowing the effect of the N additive to last longer. Thus, we found a method to sustain the effectiveness of N additive, even with low solubility. Figure 13a,c show that the capsulated $LiNO_3$ is well dissolved in the carbonate-based electrolyte, and the N compounds form an SEI layer. Figure 13b shows the fabrication process for the polymer capsule and a schematic of the resulting SEI layer. In addition, to achieve sustained dissolution of N additives with similar performance, metal–organic frameworks (MOFs) have been introduced [118]. Figure 13e shows a schematic representation of the process of $LiNO_3$ encapsulation in MOFs. Figure 13d shows the XPS spectra of the lithium metal surface of the cell utilizing the MOFs. It can be seen that the N compound is clearly dissolved in the electrolyte to form the SEI layer.

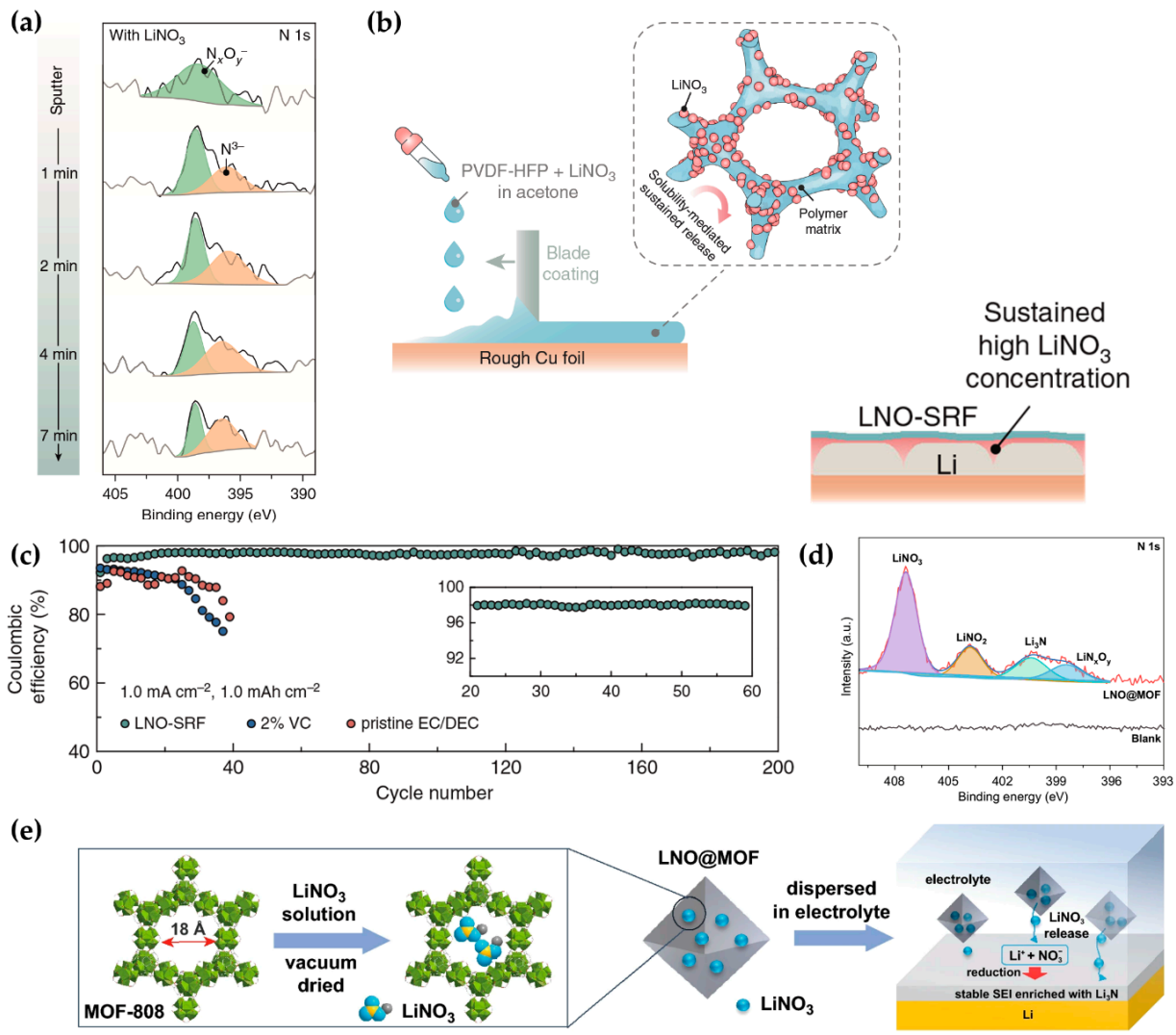


**Figure 13.** N 1s X-ray photoelectron spectroscopy (XPS) spectra confirm that the capsulated N additive is continuously soluble in the electrolyte with (**a**) polymer gel-capsulated $LiNO_3$ and (**d**) metal-organic frameworks (MOFs). Performance enhancement with capsulated N additive. (**c**) Coulombic efficiency of 1.0 M $LiPF_6$ ethylene carbonate (EC)/diethyl carbonate (DEC) electrolyte with and without $LiNO_3$ [98]. Reprinted with permission from Ref. [98]. Copyright © 2018 nature. (**b**,**e**) Schematic illustration of the two types of capsule mockups and the solid electrolyte interphases (SEIs) that are generated by polymer gel with capsuled $LiNO_3$ [118]. Reprinted with permission from Ref. [118]. Copyright © 2020 Springer Nature.

### *3.3. The New Approach in Carbonate-Based Electrolytes: Solubilizer-Free N-Based Electrolyte Additive*

As mentioned earlier, the solubility of N additives in carbonate-based electrolytes is extremely low. Therefore, attempts to dissolve N additives in carbonate-based electrolytes are ongoing, focusing on strategies that utilize solubilizers [119]. The development of 1-trimethlsilyl imidazole lithium nitrate adduct (TMSILN) is expected to provide a different direction, as it does not require the presence of other additives to increase the solubility of the N additive. This newly developed N additive improves the solubility of $LiNO_3$ salts, which are poorly soluble in carbonate-based electrolytes, allowing them to be dissolved in more than 1 M. TMSILN contains $LiNO_3$ and 1-trimethlsilylimidazole (1-TMSI) moieties, and the cationic bond between the two substances creates a $LiNO_3$ derivative that can be dissolved in a carbonate-based electrolyte, thereby increasing its solubility in the electrolyte. This study showed that the trimethylsilyl functional group in the TMSI portion can react

with the trace amount of $H_2O$ contained in the cell to inhibit the degradation of $LiPF_6$ by inhibiting HF formation and improving electrochemical performance. In this study, it is demonstrated that TMSILN-added carbonate-based electrolytes can induce uniform spherical lithium electrodeposition and form an SEI layer with N compounds, which can benefit from the effect of $LiNO_3$ to stabilize the SEI layer.

Figure 14a,b show that the TMSILN is readily soluble in 1 wt% $LiNO_3$, unlike the pure $LiNO_3$ salt, which is not soluble in more than 0.5 wt% of carbonate-based electrolyte and precipitates to the bottom. This indicates that the TMSILN salt is highly soluble in the original carbonate electrolyte, which is significantly different from the solubility of the N additive in the original carbonate electrolyte. The XPS spectra (Figure 14c,d) of the lithium metal cathode surface show that the carbonate-based electrolyte containing TMSILN contains N compounds. In addition, silicon-containing fragments of the TMSILN additive, which are expected to be included in the SEI layer, are not found because the reduction reaction of the N compound is superior to other electrolyte compositions.

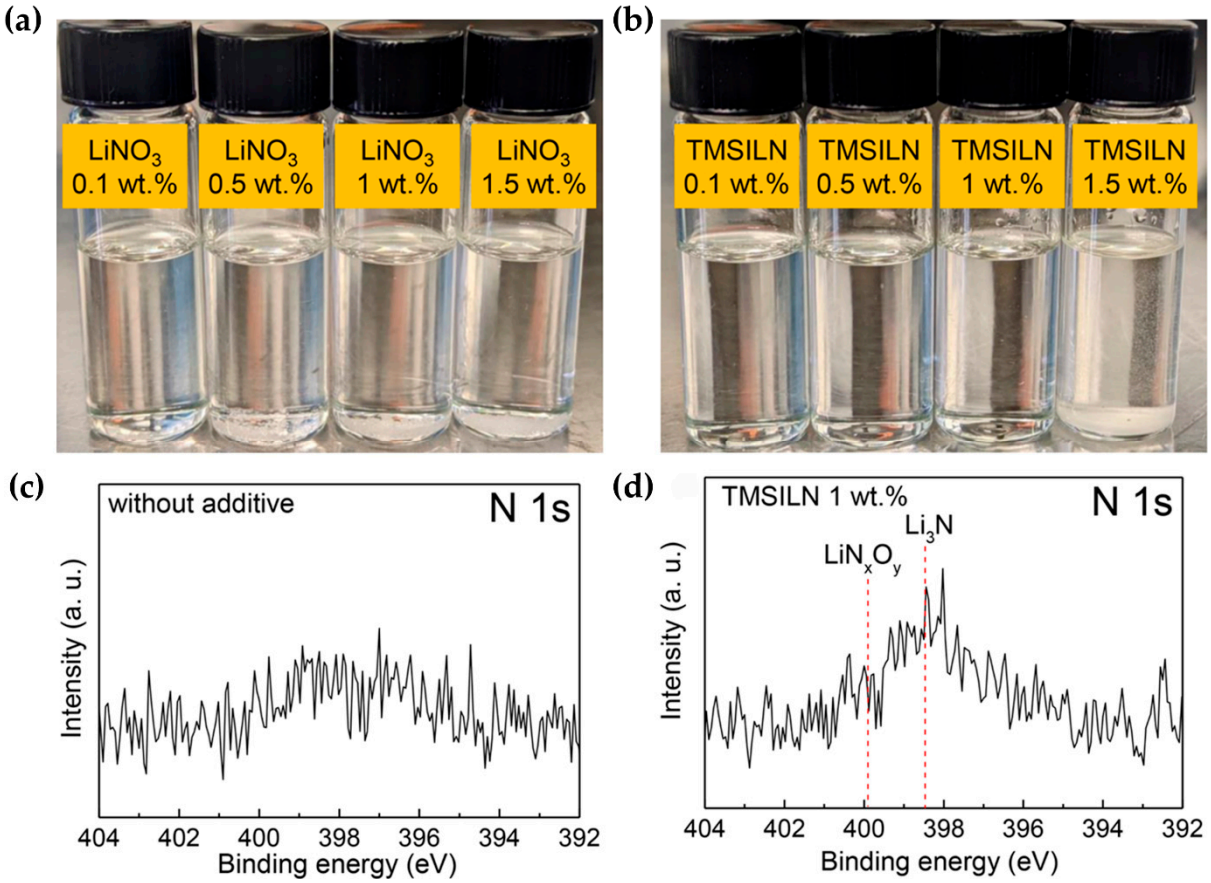


**Figure 14.** The rationale of dissolving $LiNO_3$ in carbonate electrolyte. (**a**,**b**) Photographs of pure $LiNO_3$ and 1-trimethlsilyl imidazole lithium nitrate (TMSILN) dissolved in ethylene carbonate (EC)/ethyl methyl carbonate (EMC) (3:7 vol%) electrolyte. (**c**) N 1s XPS spectra of lithium metal surface in pure EC/EMC (3:7 vol%) electrolyte, (**d**) EC/EMC (3:7 vol%) electrolyte containing 1 wt% TMSILN [119]. Reprinted with permission from Ref. [119]. Copyright © 2023 American Chemical Society.

Here, we discuss the dendrite inhibition effect of carbonate-based electrolytes containing TMSILN. Carbonate-based electrolytes with TMSILN can have a lower overvoltage and polarization and improved cycle performance compared to electrolytes without additives (Figure 15a). A comparison of the cycle stability of the cell with an ether-based electrolyte and that with a carbonate-based electrolyte containing TMSILN with a high-voltage anode (Figure 15b) shows that the carbonate-based electrolyte with TMSILN does not decompose

at the anode operating voltage. It can also be seen that the cycle performance is improved compared with that of the pure carbonate-based electrolyte. Inhomogeneous dendrites are observed on the lithium metal surface of the Li–Li cell with the carbonate electrolyte without additives (Figure 15c). However, in the electrolyte containing TMSILN, large, spherical, and uniform lithium dendritic crystal electrodeposits are observed (Figure 15d). This uniform dendrite formation can significantly reduce the risk of short circuits caused by dendrites. Thus, the TMSILN electrolyte additive, containing N compounds in the SEI layer, can fulfill the role of a N additive.

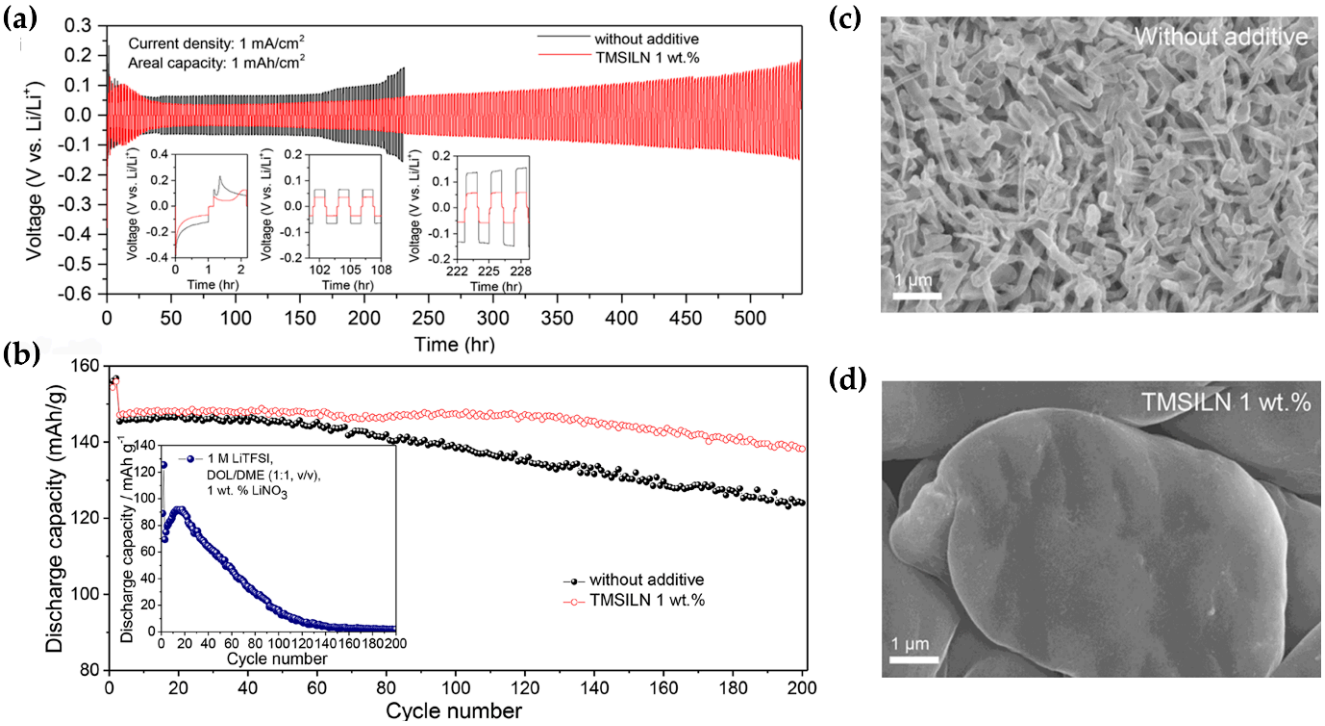


**Figure 15.** Effect of the N additive in a carbonate-based electrolyte containing 1-trimethlsilyl imidazole lithium nitrate (TMSILN). (**a**) Comparison of overvoltage graphs over time for pure carbonate-based electrolyte and carbonate-based electrolyte containing TMSILN. (**b**) Cycling performance of NCM622/Li cell with pure ethylene carbonate (EC)/ethyl metyl carbonate (EMC) (3:7 vol%) electrolyte and EC/EMC (3:7 vol%) electrolyte containing TMSILN. The graph in the lower left shows the constant current cycling performance of the NCM622/Li cell in 1 M $LiPF_6$ 1,3-dioxolane (DOL)/1,2-dimethoxyethane (DME) (1:1 $v/v$) with 1 wt% $LiNO_3$. Field emission scanning electron microscope (FE-SEM) images showing lithium electrode morphology after primary electrodeposition at 1 mA $cm^{-2}$ for 1 mAh $cm^{-2}$ in Li/Li symmetric cells applying (**c**) pure carbonate-based electrolyte and (**d**) carbonate-based electrolyte containing TMSILN [119]. Reprinted with permission from Ref. [119]. Copyright © 2023 American Chemical Society.

The development of TMSILN is significant because it shows that $LiNO_3$ additives, which have only been used alone in ether-based electrolytes, can stabilize the lithium precipitation behavior of lithium metal surfaces in carbonate-based electrolytes and can be an important indicator of the possibility of using them alone. Although it is good that several studies are being conducted to explore various possibilities using the stable state of lithium metal anodes in ether-based electrolytes, carbonate-based electrolytes are needed for commercialization, and thus further research, such as the aforementioned, should be conducted for commercialization, with this invention leading the way.

## 4. Summary and Conclusions

The main obstacle to implementing lithium metal anodes with their high theoretical capacity in batteries is the formation of lithium dendrites and the resulting electrochemical degradation and safety issues. Various strategies have been proposed to address these challenges. Among these, electrolyte additives offer a straightforward and cost-effective solution. There are many types of electrolytes, but this review focuses on ether-based and carbonate-based electrolytes. Ether-based electrolytes have the advantage of good reduction stability for lithium metal anodes. Therefore, lithium metal batteries are extensively investigated in ether-based electrolyte environments, which has led to the discovery of the potential utilization of N additives. The N additive reacts with the lithium metal anode prior to other components in the electrolyte, forming a stable SEI layer, which increases the coulombic efficiency, capacity, and stability of the lithium metal batteries. However, ether-based electrolytes are prone to decomposition because of their low oxidation stability at high voltages. Therefore, the utilization of carbonate-based electrolytes is necessary due to their more stable properties at high voltages. However, implementing this strategy is challenging. N additives demonstrate poor solubility in carbonate-based electrolytes. To address this challenge and mitigate dendrite formation on lithium metal anodes, thus making them commercially viable, extensive research efforts have been dedicated to enhancing the solubility of N additives in carbonate-based electrolytes (Table 1). Most studies have adopted the strategy of adding N additives to carbonate-based electrolytes with solubilizers. Alternatively, they dissolve the additives in any solvent with high solubility for N additives and add small amounts to carbonate-based electrolytes. However, this approach may not effectively address unexpected chemical reactions, and it can be challenging to demonstrate its potential for further development. Recently, a new approach has been reported, in which a highly soluble N additive (TMSILN) in carbonate-based electrolyte without the need for any solubilizer has been synthesized. Although this research offers a new method to increase the solubility of N additives without the need for a solubilizer, more extensive research is needed to explore such new strategies for the stable utilization of lithium metal in batteries.

**Table 1.** Comparison of properties of dual salts for solubility enhancement.

| Additive | Solubility | Capacity Retention | Coulombic Efficiency | Others | Reference |
|---|---|---|---|---|---|
| LiFSI | 2 M | 98.5% (425 cycles) | 47.3–52.7% (100 cycles) | Formation SEI with LiF-$Li_3N$-$LiN_xO_y$ on lithium metal surface | [80] |
| CuF | 1 wt% | 53% (300 cycles) | 99.5% (300 cycles) | A catalyst not participating in reactions within the battery | [97] |
| Tin(II) | 5 wt% | 89.6% (130 cycles) | 98.4% (300 cycles) | A catalyst not participating in reactions within the battery | [99] |
| CsF | 0.5 wt% | N/A | ~98% (200 cycles) | Synergy effect with SHES effect | [98] |
| Pyridine | Adding 1 wt% to a solvent dissolved in 4.5 M $LiNO_3$ | N/A | ~95.86% (80 h, 1 mAh $cm^{-2}$, 1 mA $cm^{-2}$) | High DN | [105] |
| TEGDME | 3 wt% | 87.3% (250 cycles) | 98.2% (350 cycles) | $Li^+$ ion solvation structure modification | [106] |
| GBL | 0.5 M | ~80% (100 cycles) | ~98.8% (200 cycles) | High DN $Li^+$ ion solvation structure modification | [109] |
| TMSILN | 1 wt% | 90% (300 cycles) | N/A | Lithium nitrate-containing salt. No required additional additives | [117] |

**Author Contributions:** Conceptualization, J.K. and O.B.C.; writing—original draft preparation, J.K.; writing—review and editing, T.Y. and O.B.C.; Supervision, O.B.C. All authors have read and agreed to the published version of the manuscript.

**Funding:** This work was supported by the Gachon University research fund of 2023 (GCU-202400930001). This work was also supported by the Technology Innovation Program (20025626) funded by the Ministry of Trade, Industry & Energy (MOTIE, Republic of Korea).

**Conflicts of Interest:** The authors declare no conflicts of interest.

## References

1. Winter, M.; Brodd, R.J. What are batteries, fuel cells, and supercapacitors? *Chem. Rev.* **2004**, *104*, 4245–4270. [CrossRef]
2. Seok, J.; Lee, W.; Lee, H.; Park, S.; Chung, C.; Hwang, S.; Yoon, W.-S. Aging Mechanisms of Lithium-ion Batteries. *J. Electrochem. Sci. Technol.* **2024**, *15*, 51–66. [CrossRef]
3. Salunkhe, T.T.; Kadam, A.N.; Hur, J.; Kim, I.T. Green and sustainably designed intercalation-type anodes for emerging lithium dual-ion batteries with high energy density. *J. Energy Chem.* **2023**, *80*, 466–478. [CrossRef]
4. Huy, V.P.H.; So, S.; Kim, I.T.; Hur, J. Self-healing gallium phosphide embedded in a hybrid matrix for high-performance Li-ion batteries. *Energy Storage Mater.* **2021**, *34*, 669–681. [CrossRef]
5. Salunkhe, T.T.; Varma, R.S.; Kadam, A.N.; Lee, S.W.; Lee, Y.C.; Hur, J.; Kim, I.T. Scraps to superior anodes for Li-ion batteries: Sustainable and scalable upgrading of waste rust. *J. Hazard. Mater.* **2021**, *410*, 124571. [CrossRef] [PubMed]
6. Kim, D.S.; Bae, J.; Kwon, S.H.; Hur, J.; Lee, S.G.; Kim, I.T. Synergistic effect of antimony-triselenide on addition of conductive hybrid matrix for high-performance lithium-ion batteries. *J. Alloys Compd.* **2020**, *828*, 154410. [CrossRef]
7. Lee, J.H.; Kang, S.G.; Kim, I.T.; Kwon, S.; Lee, I.; Lee, S.G. Adsorption mechanisms of lithium oxides ($Li_xO_2$) on N-doped graphene: A density functional theory study with implications for lithium-air batteries. *Theor. Chem. Acc.* **2016**, *135*, 193–202. [CrossRef]
8. Lim, Y.E.; Choi, W.S.; Kim, J.H.; Ahn, Y.N.; Kim, I. The Sn-red P-Fe-based alloy materials for efficient Li-ion battery anodes. *J. Ind. Eng. Chem.* **2023**, *121*, 299–311. [CrossRef]
9. Kim, H.; Kim, D.I.; Yoon, W.S. Enhancing Electrochemical Performance of $Co(OH)_2$ Anode Materials by Introducing Graphene for Next-Generation Li-ion Batteries. *J. Electrochem. Sci. Technol.* **2022**, *13*, 398–406. [CrossRef]
10. Tran, Q.N.; Park, C.H.; Le, T.H. Nanocrystalline Cellulose-Supported Iron Oxide Composite Materials for High-Performance Lithium-Ion Batteries. *Polymers* **2024**, *16*, 691. [CrossRef]
11. Sin, D.H.; Kim, S.H.; Lee, J.; Lee, H. Modification of Electrode Interface with Fullerene-Based Self-Assembled Monolayer for High-Performance Organic Optoelectronic Devices. *Micromachines* **2022**, *13*, 1613. [CrossRef] [PubMed]
12. Blomgren, G.E. The Development and Future of Lithium Ion Batteries. *J. Electrochem. Soc.* **2017**, *164*, A5019–A5025. [CrossRef]
13. Armand, M.; Tarascon, J.M. Building better batteries. *Nature* **2008**, *451*, 652–657. [CrossRef] [PubMed]
14. Sasaki, T.; Ukyo, Y.; Novák, P. Memory effect in a lithium-ion battery. *Nat. Mater.* **2013**, *12*, 569–575. [CrossRef] [PubMed]
15. Chagas, L.G.; Jeong, S.; Hasa, I.; Passerini, S. Ionic Liquid-Based Electrolytes for Sodium-Ion Batteries: Tuning Properties to Enhance the Electrochemical Performance of Manganese-Based Layered Oxide Cathode. *ACS Appl. Mater. Interfaces* **2019**, *11*, 22278–22289. [CrossRef] [PubMed]
16. Lu, D.P.; Tao, J.H.; Yan, P.F.; Henderson, W.A.; Li, Q.Y.; Shao, Y.Y.; Helm, M.L.; Borodin, O.; Graff, G.L.; Polzin, B.; et al. Formation of Reversible Solid Electrolyte Interface on Graphite Surface from Concentrated Electrolytes. *Nano Lett.* **2017**, *17*, 1602–1609. [CrossRef] [PubMed]
17. Xu, W.; Wang, J.; Ding, F.; Chen, X.; Nasybulin, E.; Zhang, Y.; Zhang, J.-G. Lithium metal anodes for rechargeable batteries. *Energy Environ. Sci.* **2014**, *7*, 513–537. [CrossRef]
18. Kim, H.; Kim, D.I.; Yoon, W.S. Challenges and Design Strategies for Conversion-Based Anode Materials for Lithium- and Sodium-Ion Batteries. *J. Electrochem. Sci. Technol.* **2022**, *13*, 32–53. [CrossRef]
19. Janek, J.; Zeier, W.G. A solid future for battery development. *Nat. Energy* **2016**, *1*, 16141. [CrossRef]
20. Yamada, Y.; Usui, K.; Chiang, C.H.; Kikuchi, K.; Furukawa, K.; Yamada, A. General Observation of Lithium Intercalation into Graphite in Ethylene-Carbonate-Free Superconcentrated Electrolytes. *ACS Appl. Mater. Interfaces* **2014**, *6*, 10892–10899. [CrossRef]
21. Lin, D.; Liu, Y.; Cui, Y. Reviving the lithium metal anode for high-energy batteries. *Nat. Nanotechnol.* **2017**, *12*, 194–206. [CrossRef] [PubMed]
22. Zhang, J.G. Anode-less. *Nat. Energy* **2019**, *4*, 637–638. [CrossRef]
23. Wang, R.H.; Cui, W.S.; Chu, F.L.; Wu, F.X. Lithium metal anodes: Present and future. *J. Energy Chem.* **2020**, *48*, 145–159. [CrossRef]
24. Zhang, Y.; Zuo, T.T.; Popovic, J.; Lim, K.; Yin, Y.X.; Maier, J.; Guo, Y.G. Towards better Li metal anodes: Challenges and strategies. *Mater. Today* **2020**, *33*, 56–74. [CrossRef]
25. Cheng, X.B.; Zhang, R.; Zhao, C.Z.; Zhang, Q. Toward Safe Lithium Metal Anode in Rechargeable Batteries: A Review. *Chem. Rev.* **2017**, *117*, 10403–10473. [CrossRef] [PubMed]
26. Tarascon, J.M.; Armand, M. Issues and challenges facing rechargeable lithium batteries. *Nature* **2001**, *414*, 359–367. [CrossRef] [PubMed]

27. Yang, C.P.; Fu, K.; Zhang, Y.; Hitz, E.; Hu, L.B. Protected Lithium-Metal Anodes in Batteries: From Liquid to Solid. *Adv. Mater.* **2017**, *29*, 1701169. [CrossRef] [PubMed]
28. He, X.F.; Liu, X.; Han, Q.; Zhang, P.; Song, X.S.; Zhao, Y. A Liquid/Liquid Electrolyte Interface that Inhibits Corrosion and Dendrite Growth of Lithium in Lithium-Metal Batteries. *Angew. Chem. Int. Ed.* **2020**, *59*, 6397–6405. [CrossRef] [PubMed]
29. Zhang, X.Q.; Cheng, X.B.; Chen, X.; Yan, C.; Zhang, Q. Fluoroethylene Carbonate Additives to Render Uniform Li Deposits in Lithium Metal Batteries. *Adv. Funct. Mater.* **2017**, *27*, 1605989. [CrossRef]
30. Chae, O.B.; Adiraju, V.A.K.; Lucht, B.L. Lithium Cyano Tris(2,2,2-trifluoroethyl) Borate as a Multifunctional Electrolyte Additive for High-Performance Lithium Metal Batteries. *ACS Energy Lett.* **2021**, *6*, 3851–3857. [CrossRef]
31. Wang, S.H.; Yin, Y.X.; Zuo, T.T.; Dong, W.; Li, J.Y.; Shi, J.L.; Zhang, C.H.; Li, N.W.; Li, C.J.; Guo, Y.G. Stable Li Metal Anodes via Regulating Lithium Plating/Stripping in Vertically Aligned Microchannels. *Adv. Mater.* **2017**, *29*, 1703729. [CrossRef] [PubMed]
32. Yang, C.P.; Yin, Y.X.; Zhang, S.F.; Li, N.W.; Guo, Y.G. Accommodating lithium into 3D current collectors with a submicron skeleton towards long-life lithium metal anodes. *Nat. Commun.* **2015**, *6*, 8058. [CrossRef]
33. Liu, Y.Y.; Lin, D.C.; Yuen, P.Y.; Liu, K.; Xie, J.; Dauskardt, R.H.; Cui, Y. An Artificial Solid Electrolyte Interphase with High Li-Ion Conductivity, Mechanical Strength, and Flexibility for Stable Lithium Metal Anodes. *Adv. Mater.* **2017**, *29*, 1605531. [CrossRef] [PubMed]
34. Li, N.W.; Shi, Y.; Yin, Y.X.; Zeng, X.X.; Li, J.Y.; Li, C.J.; Wan, L.J.; Wen, R.; Guo, Y.G. A Flexible Solid Electrolyte Interphase Layer for Long-Life Lithium Metal Anodes. *Angew. Chem. Int. Ed.* **2018**, *57*, 1505–1509. [CrossRef] [PubMed]
35. Li, P.L.; Dong, X.L.; Li, C.; Liu, J.Y.; Liu, Y.; Feng, W.L.; Wang, C.X.; Wang, Y.G.; Xia, Y.Y. Anchoring an Artificial Solid-Electrolyte Interphase Layer on a 3D Current Collector for High-Performance Lithium Anodes. *Angew. Chem. Int. Ed.* **2019**, *58*, 2093–2097. [CrossRef] [PubMed]
36. Liang, J.Y.; Zhang, X.D.; Zeng, X.X.; Yan, M.; Yin, Y.X.; Xin, S.; Wang, W.P.; Wu, X.W.; Shi, J.L.; Wan, L.J.; et al. Enabling a Durable Electrochemical Interface via an Artificial Amorphous Cathode Electrolyte Interphase for Hybrid Solid/Liquid Lithium-Metal Batteries. *Angew. Chem. Int. Ed.* **2020**, *59*, 6585–6589. [CrossRef]
37. Monroe, C.; Newman, J. The impact of elastic deformation on deposition kinetics at lithium/polymer interfaces. *J. Electrochem. Soc.* **2005**, *152*, A396–A404. [CrossRef]
38. Kim, Y.; Stepien, D.; Moon, H.; Schönherr, K.; Schumm, B.; Kuenzel, M.; Althues, H.; Bresser, D.; Passerini, S. Artificial Interphase Design Employing Inorganic-Organic Components for High-Energy Lithium-Metal Batteries. *ACS Appl. Mater. Interfaces* **2023**, *15*, 20987–20997. [CrossRef] [PubMed]
39. Lee, D.; Sun, S.; Park, H.; Kim, J.; Park, K.; Hwang, I.; Jung, Y.; Song, T.; Paik, U. Stable artificial solid electrolyte interphase with lithium selenide and lithium chloride for dendrite-free lithium metal anodes. *J. Power Sources* **2021**, *506*, 230158. [CrossRef]
40. Zuo, T.T.; Wu, X.W.; Yang, C.P.; Yin, Y.X.; Ye, H.; Li, N.W.; Guo, Y.G. Graphitized Carbon Fibers as Multifunctional 3D Current Collectors for High Areal Capacity Li Anodes. *Adv. Mater.* **2017**, *29*, 1700389. [CrossRef]
41. Ma, Q.; Zeng, X.X.; Yue, J.P.; Yin, Y.X.; Zuo, T.T.; Liang, J.Y.; Deng, Q.; Wu, X.W.; Guo, Y.G. Viscoelastic and Nonflammable Interface Design-Enabled Dendrite-Free and Safe Solid Lithium Metal Batteries. *Adv. Energy Mater.* **2019**, *9*, 1803854. [CrossRef]
42. Jaumaux, P.; Liu, Q.; Zhou, D.; Xu, X.F.; Wang, T.Y.; Wang, Y.Z.; Kang, F.Y.; Li, B.H.; Wang, G.X. Deep-Eutectic-Solvent-Based Self-Healing Polymer Electrolyte for Safe and Long-Life Lithium-Metal Batteries. *Angew. Chem. Int. Ed.* **2020**, *59*, 9134–9142. [CrossRef]
43. Lee, J.; Heo, K.; Song, Y.W.; Hwang, D.; Kim, M.Y.; Jeong, H.; Shin, D.C.; Lim, J. Degradation of All-Solid-State Lithium-Sulfur Batteries with PEO-Based Composite Electrolyte. *J. Electrochem. Sci. Technol.* **2022**, *13*, 199–207. [CrossRef]
44. Zhang, S.S. Role of $LiNO_3$ in rechargeable lithium/sulfur battery. *Electrochim. Acta* **2012**, *70*, 344–348. [CrossRef]
45. Shi, Q.W.; Zhong, Y.R.; Wu, M.; Wang, H.Z.; Wang, H.L. High-capacity rechargeable batteries based on deeply cyclable lithium metal anodes. *Proc. Natl. Acad. Sci. USA* **2018**, *115*, 5676–5680. [CrossRef]
46. Wang, H.S.; Liu, Y.Y.; Li, Y.Z.; Cui, Y. Lithium Metal Anode Materials Design: Interphase and Host. *Electrochem. Energy Rev.* **2019**, *2*, 509–517. [CrossRef]
47. Jäckle, M.; Gross, A. Microscopic properties of lithium, sodium, and magnesium battery anode materials related to possible dendrite growth. *J. Chem. Phys.* **2014**, *141*, 4701. [CrossRef]
48. Kim, S.; Park, G.; Lee, S.J.; Seo, S.; Ryu, K.; Kim, C.H.; Choi, J.W. Lithium-Metal Batteries: From Fundamental Research to Industrialization. *Adv. Mater.* **2023**, *35*, 2206625. [CrossRef]
49. Han, Y.Y.; Liu, B.; Xiao, Z.; Zhang, W.K.; Wang, X.L.; Pan, G.X.; Xia, Y.; Xia, X.H.; Tu, J.P. Interface issues of lithium metal anode for high-energy batteries: Challenges, strategies, and perspectives. *InfoMat* **2021**, *3*, 155–174. [CrossRef]
50. Chae, O.B.; Lucht, B.L. Interfacial Issues and Modification of Solid Electrolyte Interphase for Li Metal Anode in Liquid and Solid Electrolytes. *Adv. Energy Mater.* **2023**, *13*, 2203791. [CrossRef]
51. Yuan, W.J.; Chen, J.; Shi, G.Q. Nanoporous graphene materials. *Mater. Today* **2014**, *17*, 77–85. [CrossRef]
52. Amanchukwu, C.V.; Yu, Z.; Kong, X.; Qin, J.; Cui, Y.; Bao, Z.N. A New Class of Ionically Conducting Fluorinated Ether Electrolytes with High Electrochemical Stability. *J. Am. Chem. Soc.* **2020**, *142*, 7393–7403. [CrossRef]
53. Sun, S.; Kim, G.; Lee, D.; Park, E.; Myeong, S.; Son, B.; Lee, K.; Jang, M.; Paik, U.; Song, T. Modulating SEI formation via tuning the solvation sheath for lithium metal batteries. *Chem. Commun.* **2022**, *58*, 9834–9837. [CrossRef] [PubMed]
54. Aslam, M.K.; Niu, Y.B.; Hussain, T.; Tabassum, H.; Tang, W.W.; Xu, M.W.; Ahuja, R. How to avoid dendrite formation in metal batteries: Innovative strategies for dendrite suppression. *Nano Energy* **2021**, *86*, 106142. [CrossRef]

55. Goodenough, J.B.; Park, K.S. The Li-Ion Rechargeable Battery: A Perspective. *J. Am. Chem. Soc.* **2013**, *135*, 1167–1176. [CrossRef]
56. Fu, L.; Wang, X.C.; Chen, Z.H.; Li, Y.J.; Mao, E.Y.; Seh, Z.W.; Sun, Y.M. Insights on "nitrate salt" in lithium anode for stabilized solid electrolyte interphase. *Carbon Energy* **2022**, *4*, 12–20. [CrossRef]
57. Liu, S.F.; Ji, X.; Piao, N.; Chen, J.; Eidson, N.; Xu, J.J.; Wang, P.F.; Chen, L.; Zhang, J.X.; Deng, T.; et al. An Inorganic-Rich Solid Electrolyte Interphase for Advanced Lithium-Metal Batteries in Carbonate Electrolytes. *Angew. Chem. Int. Ed.* **2021**, *60*, 3661–3671. [CrossRef]
58. Huang, S.Z.; Huang, Y.P.; Xia, Y.J.; Ding, J.Y.; Peng, C.Y.; Wang, L.L.; Luo, J.R.; Zhang, X.X.; Zheng, J.R.; Gao, Y.Q.; et al. High $Li^+$ coordinated solvation sheaths enable high-quality Li metal anode. *InfoMat* **2023**, *5*, e12411. [CrossRef]
59. Fu, L.; Wang, X.C.; Wang, L.; Wan, M.T.; Li, Y.J.; Cai, Z.; Tan, Y.C.; Li, G.C.; Zhan, R.M.; Seh, Z.W.; et al. A Salt-in-Metal Anode: Stabilizing the Solid Electrolyte Interphase to Enable Prolonged Battery Cycling. *Adv. Funct. Mater.* **2021**, *31*, 2010602. [CrossRef]
60. Hou, L.P.; Yao, N.; Xie, J.; Shi, P.; Sun, S.Y.; Jin, C.B.; Chen, C.M.; Liu, Q.B.; Li, B.Q.; Zhang, X.Q.; et al. Modification of Nitrate Ion Enables Stable Solid Electrolyte Interphase in Lithium Metal Batteries. *Angew. Chem. Int. Ed.* **2022**, *61*, e202201406. [CrossRef]
61. Wang, Q.D.; Yao, Z.P.; Zhao, C.L.; Verhallen, T.; Tabor, D.P.; Liu, M.; Ooms, F.; Kang, F.Y.; Aspuru-Guzik, A.; Hu, Y.S.; et al. Interface chemistry of an amide electrolyte for highly reversible lithium metal batteries. *Nat. Commun.* **2020**, *11*, 4188. [CrossRef]
62. Aurbach, D.; Pollak, E.; Elazari, R.; Salitra, G.; Kelley, C.S.; Affinito, J. On the Surface Chemical Aspects of Very High Energy Density, Rechargeable Li-Sulfur Batteries. *J. Electrochem. Soc.* **2009**, *156*, A694–A702. [CrossRef]
63. Luo, D.; Li, M.; Zheng, Y.; Ma, Q.; Gao, R.; Zhang, Z.; Dou, H.; Wen, G.; Shui, L.; Yu, A.; et al. Electrolyte Design for Lithium Metal Anode-Based Batteries toward Extreme Temperature Application. *Adv. Sci.* **2021**, *8*, 2101051. [CrossRef]
64. Alpen, U.V. $Li_3N$: A Promising Li Ionic Conductor. *J. Solid State Chem.* **1979**, *29*, 379–392. [CrossRef]
65. Heinz Schulz, K.H.T. Defect Structure of the Ionic Conductor Lithium Nitride. *Acta Crystallogr. Sect. A Cryst. Phys. Diffr. Theor. Gen. Crystallogr.* **1979**, *35*, 309–314. [CrossRef]
66. LAPP, T.; Skaarup, S.; Hooper, A. Ionic conductivity of pure and doped $Li_3N$. *Solid State Ion.* **1983**, *11*, 97–103. [CrossRef]
67. Kowada, Y.; Tatsumisago, M.; Minami, T. Chemical bonding and lithium ion conductions in $Li_3N$. *Solid State Ion.* **2009**, *180*, 462–466. [CrossRef]
68. Lee, H.S.; Bin Lee, S.; Kim, Y.S.; Kim, H.; Kim, M.J.; Yoon, T.W.; Lee, D.K.; Cho, J.H.; Kim, Y.H.; Kang, B.S. Boosting thermoelectric performance of conjugated polymers via interchain molecular docking: Significance of highly crystalline and percolated morphology. *Chem. Eng. J.* **2023**, *468*, 143654. [CrossRef]
69. Kanwal, S.; Rahman, G. Defects-driven magnetism in bulk $\alpha$-$Li_3N$. *J. Magn. Magn. Mater.* **2018**, *466*, 192–199. [CrossRef]
70. Li, W.; Wu, G.; Araújo, C.M.; Scheicher, R.H.; Blomqvist, A.; Ahuja, R.; Xiong, Z.; Feng, Y.; Chen, P. $Li^+$ ion conductivity and diffusion mechanism in $\alpha$-$Li_3N$ and $\beta$-$Li_3N$. *Energy Environ. Sci.* **2010**, *3*, 1524–1530. [CrossRef]
71. Lee, H.; Li, H.; Kim, Y.S.; Park, S.M.; Lee, D.; Lee, S.; Lee, H.S.; Kim, Y.H.; Kang, B. Novel Dithienopyrrole-Based Conjugated Copolymers: Importance of Backbone Planarity in Achieving High Electrical Conductivity and Thermoelectric Performance. *Macromol. Rapid Commun.* **2022**, *43*, 2200277. [CrossRef]
72. Li, T.; Li, Y.; Sun, Y.L.; Qian, Z.F.; Wang, R.H. New Insights on the Good Compatibility of Ether-Based Localized High-Concentration Electrolyte with Lithium Metal. *ACS Mater. Lett.* **2021**, *3*, 838–844. [CrossRef]
73. Ren, X.D.; Zou, L.F.; Jiao, S.H.; Mei, D.H.; Engelhard, M.H.; Li, Q.Y.; Lee, H.Y.; Niu, C.J.; Adams, B.D.; Wang, C.M.; et al. High-Concentration Ether Electrolytes for Stable High-Voltage Lithium Metal Batteries. *ACS Energy Lett.* **2019**, *4*, 896–902. [CrossRef]
74. Jozwiuk, A.; Sommer, H.; Janek, J.; Brezesinski, T. Fair performance comparison of different carbon blacks in lithium-sulfur batteries with practical mass loadings-Simple design competes with complex cathode architecture. *J. Power Sources* **2015**, *296*, 454–461. [CrossRef]
75. Jozwiuk, A.; Berkes, B.B.; Weiss, T.; Sommer, H.; Janek, J.; Brezesinski, T. The critical role of lithium nitrate in the gas evolution of lithium-sulfur batteries. *Energy Environ. Sci.* **2016**, *9*, 2603–2608. [CrossRef]
76. Morgan, B.; Madden, P.A. Ion mobilities and microscopic dynamics in liquid (Li,K)Cl. *J. Chem. Phys.* **2004**, *120*, 1402–1413. [CrossRef]
77. Davoodabadi, A.; Li, J.L.; Liang, Y.F.; Wood, D.L.; Singler, T.J.; Jin, C.R. Analysis of electrolyte imbibition through lithium-ion battery electrodes. *J. Power Sources* **2019**, *424*, 193–203. [CrossRef]
78. Warrington, A.; Hasanpoor, M.; Balkis, A.; Howlett, P.C.; Hutt, O.E.; Forsyth, M.; Pringle, J.M. Investigation of properties and performance of three novel highly concentrated ether-functionalised ionic liquid electrolytes for lithium metal batteries. *Energy Storage Mater.* **2023**, *63*, 102984. [CrossRef]
79. Adams, B.D.; Carino, E.V.; Connell, J.G.; Han, K.S.; Cao, R.; Chen, J.; Zheng, J.; Li, Q.; Mueller, K.T.; Henderson, W.A.; et al. Long term stability of Li-S batteries using high concentration lithium nitrate electrolytes. *Nano Energy* **2017**, *40*, 607–617. [CrossRef]
80. Zhang, X.Z.; Lin, X.D.; Xu, P.; Yuan, R.M.; Gupta, D.; Rupp, R.; Barozzino-Consiglio, G.; Xu, H.W.; Dong, Q.F.; Vlad, A. Strong ion pairing at the origin of modified Li-cation solvation and improved performances of dual-salt electrolytes. *J. Power Sources* **2022**, *541*, 231644. [CrossRef]
81. Zhang, X.Q.; Chen, X.; Hou, L.P.; Li, B.Q.; Cheng, X.B.; Huang, J.Q.; Zhang, Q. Regulating Anions in the Solvation Sheath of Lithium Ions for Stable Lithium Metal Batteries. *ACS Energy Lett.* **2019**, *4*, 411–416. [CrossRef]

82. Kang, D.W.; Moon, J.; Choi, H.-Y.; Shin, H.-C.; Kim, B.G. Stable cycling and uniform lithium deposition in anode-free lithium-metal batteries enabled by a high-concentration dual-salt electrolyte with high $LiNO_3$ content. *J. Power Sources* **2021**, *490*, 229504. [CrossRef]
83. Rodriguez, R.; Edison, R.A.; Stephens, R.M.; Sun, H.-H.; Heller, A.; Mullins, C.B. Separator-free and concentrated $LiNO_3$ electrolyte cells enable uniform lithium electrodeposition. *J. Mater. Chem. A* **2020**, *8*, 3999–4006. [CrossRef]
84. Li, W.; Yao, H.; Yan, K.; Zheng, G.; Liang, Z.; Chiang, Y.-M.; Cui, Y. The synergetic effect of lithium polysulfide and lithium nitrate to prevent lithium dendrite growth. *Nat. Commun.* **2015**, *6*, 7436. [CrossRef] [PubMed]
85. Xiong, S.; Xie, K.; Diao, Y.; Hong, X. Characterization of the solid electrolyte interphase on lithium anode for preventing the shuttle mechanism in lithium–sulfur batteries. *J. Power Sources* **2014**, *246*, 840–845. [CrossRef]
86. Yang, X.F.; Sun, Q.; Zhao, C.T.; Gao, X.J.; Adair, K.; Zhao, Y.; Luo, J.; Lin, X.T.; Liang, J.N.; Huang, H.; et al. Self-healing electrostatic shield enabling uniform lithium deposition in all-solid-state lithium batteries. *Energy Storage Mater.* **2019**, *22*, 194–199. [CrossRef]
87. Ding, F.; Xu, W.; Graff, G.L.; Zhang, J.; Sushko, M.L.; Chen, X.L.; Shao, Y.Y.; Engelhard, M.H.; Nie, Z.M.; Xiao, J.; et al. Dendrite-Free Lithium Deposition via Self-Healing Electrostatic Shield Mechanism. *J. Am. Chem. Soc.* **2013**, *135*, 4450–4456. [CrossRef] [PubMed]
88. Kim, Y.; Park, J.; Hwang, Y.; Jung, C. Review on Effective Skills to Inhibit Dendrite Growth for Stable Lithium Metal Electrode. *J. Korean Electrochem. Soc.* **2022**, *25*, 51–68. [CrossRef]
89. Lin, H.; Chen, K.H.; Shuai, Y.; He, X.; Ge, K. Influence of $CsNO_3$ as electrolyte additive on electrochemical property of lithium anode in rechargeable battery. *J. Cent. South Univ.* **2018**, *25*, 719–728. [CrossRef]
90. Jung, J.; Cho, H.; Kim, I.; Kim, S.; Jo, W.; Kim, H.T. Dual Functionalities of Rb Cation in Lean Electrolyte Lithium Sulfur Batteries. *Energy Storage Mater.* **2023**, *63*, 103040. [CrossRef]
91. Jia, W.S.; Fan, C.; Wang, L.P.; Wang, Q.J.; Zhao, M.J.; Zhou, A.J.; Li, J.Z. Extremely Accessible Potassium Nitrate ($KNO_3$) as the Highly Efficient Electrolyte Additive in Lithium Battery. *ACS Appl. Mater. Interfaces* **2016**, *8*, 15399–15405. [CrossRef] [PubMed]
92. Xu, Q.; Yang, Y.F.; Shao, H.X. Enhanced cycleability and dendrite-free lithium deposition by adding potassium ion to the electrolyte for lithium metal batteries. *Electrochim. Acta* **2016**, *212*, 758–766. [CrossRef]
93. Shuai, Y.; Zhang, Z.; Chen, K.; Lou, J.; Wang, Y. Highly stable lithium plating by a multifunctional electrolyte additive in a lithium-sulfurized polyacrylonitrile battery. *Chem. Commun.* **2019**, *55*, 2376–2379. [CrossRef] [PubMed]
94. Hu, L.B.; Zhang, Z.C.; Amine, K. Electrochemical investigation of carbonate-based electrolytes for high voltage lithium-ion cells. *J. Power Sources* **2013**, *236*, 175–180. [CrossRef]
95. Delp, S.A.; Borodin, O.; Olguin, M.; Eisner, C.G.; Allen, J.L.; Jow, T.R. Importance of Reduction and Oxidation Stability of High Voltage Electrolytes and Additives. *Electrochim. Acta* **2016**, *209*, 498–510. [CrossRef]
96. Borodin, O.; Behl, W.; Jow, T.R. Oxidative Stability and Initial Decomposition Reactions of Carbonate, Sulfone, and Alkyl Phosphate-Based Electrolytes. *J. Phys. Chem. C* **2013**, *117*, 8661–8682. [CrossRef]
97. Suo, L.M.; Xue, W.J.; Gobet, M.; Greenbaum, S.G.; Wang, C.; Chen, Y.M.; Yang, W.L.; Li, Y.X.; Li, J. Fluorine-donating electrolytes enable highly reversible 5-V-class Li metal batteries. *Proc. Natl. Acad. Sci. USA* **2018**, *115*, 1156–1161. [CrossRef]
98. Liu, Y.; Lin, D.; Li, Y.; Chen, G.; Pei, A.; Nix, O.; Li, Y.; Cui, Y. Solubility-mediated sustained release enabling nitrate additive in carbonate electrolytes for stable lithium metal anode. *Nat. Commun.* **2018**, *9*, 3656. [CrossRef]
99. Yan, C.; Yao, Y.-X.; Chen, X.; Cheng, X.-B.; Zhang, X.-Q.; Huang, J.-Q.; Zhang, Q. Lithium Nitrate Solvation Chemistry in Carbonate Electrolyte Sustains High-Voltage Lithium Metal Batteries. *Angew. Chem. Int. Ed.* **2018**, *57*, 14055–14059. [CrossRef]
100. Zhao, J.; Wan, Z.W.; Zeng, X.M.; Tian, M.M.; Wang, K.; Chen, X.Y.; Ling, M.; Ni, W.B.; Liang, C.D. Solubilized $LiNO_3$ by the cationic size effect of CsF for lithium metal anode protection and dendrite formation prevention in carbonate electrolyte. *Inorg. Chem. Front.* **2023**, *10*, 1809–1817. [CrossRef]
101. Zhang, W.D.; Wu, Q.; Huang, J.X.; Fan, L.; Shen, Z.Y.; He, Y.; Feng, Q.; Zhu, G.N.; Lu, Y.Y. Colossal Granular Lithium Deposits Enabled by the Grain-Coarsening Effect for High-Efficiency Lithium Metal Full Batteries. *Adv. Mater.* **2020**, *32*, 2001740. [CrossRef] [PubMed]
102. Zhang, W.D.; Shen, Z.Y.; Li, S.Y.; Fan, L.; Wang, X.Y.; Chen, F.; Zang, X.X.; Wu, T.; Ma, F.Y.; Lu, Y.Y. Engineering Wavy-Nanostructured Anode Interphases with Fast Ion Transfer Kinetics: Toward Practical Li-Metal Full Batteries. *Adv. Funct. Mater.* **2020**, *30*, 2003800. [CrossRef]
103. Xia, H.Y.; Wang, Y.K.; Fu, Z.W. Activation of trace $LiNO_3$ additives by $BF_3$ in high-concentration electrolytes towards stable lithium metal batteries. *Chem. Commun.* **2023**, *59*, 8680–8683. [CrossRef] [PubMed]
104. Zhong, J.; Wang, Z.X.; Yi, X.L.; Li, X.H.; Guo, H.J.; Peng, W.J.; Wang, J.X.; Yan, G.C. Breaking the Solubility Limit of $LiNO_3$ in Carbonate Electrolyte Assisted by $BF_3$ to Construct a Stable SEI Film for Dendrite-Free Lithium Metal Batteries. *Small* **2023**, *20*, 2308678. [CrossRef] [PubMed]
105. Li, S.Y.; Zhang, W.D.; Wu, Q.; Fan, L.; Wang, X.Y.; Wang, X.; Shen, Z.Y.; He, Y.; Lu, Y.Y. Synergistic Dual-Additive Electrolyte Enables Practical Lithium-Metal Batteries. *Angew. Chem. Int. Ed.* **2020**, *59*, 14935–14941. [CrossRef] [PubMed]
106. Wang, Z.; Wang, Y.; Wu, C.; Pang, W.K.; Mao, J.; Guo, Z. Constructing nitrided interfaces for stabilizing Li metal electrodes in liquid electrolytes. *Chem. Sci.* **2021**, *12*, 8945–8966. [CrossRef] [PubMed]
107. Liu, D.D.; Xiong, X.H.; Liang, Q.W.; Wu, X.W.; Fu, H.K. An inorganic-rich SEI induced by $LiNO_3$ additive for a stable lithium metal anode in carbonate electrolyte. *Chem. Commun.* **2021**, *57*, 9232–9235. [CrossRef] [PubMed]

108. Xiao, D.J.; Li, Q.; Luo, D.; Li, G.R.; Liu, H.; Shui, L.L.; Gourley, S.; Zhou, G.F.; Wang, X.; Chen, Z.W. Regulating the $Li^+$-Solvation Structure of Ester Electrolyte for High-Energy-Density Lithium Metal Batteries. *Small* **2020**, *16*, 2004688. [CrossRef] [PubMed]
109. Zhang, S.M.; Yang, G.J.; Liu, Z.P.; Li, X.Y.; Wang, X.F.; Chen, R.J.; Wu, F.; Wang, Z.X.; Chen, L.Q. Competitive Solvation Enhanced Stability of Lithium Metal Anode in Dual-Salt Electrolyte. *Nano Lett.* **2021**, *21*, 3310–3317. [CrossRef]
110. Brown, Z.L.; Heiskanen, S.; Lucht, B.L. Using Triethyl Phosphate to Increase the Solubility of $LiNO_3$ in Carbonate Electrolytes for Improving the Performance of the Lithium Metal Anode. *J. Electrochem. Soc.* **2019**, *166*, A2523–A2527. [CrossRef]
111. Jie, Y.; Liu, X.; Lei, Z.; Wang, S.; Chen, Y.; Huang, F.; Cao, R.; Zhang, G.; Jiao, S. Enabling High-Voltage Lithium Metal Batteries by Manipulating Solvation Structure in Ester Electrolyte. *Angew. Chem. Int. Ed.* **2020**, *59*, 3505–3510. [CrossRef]
112. Zhang, X.; Chen, X.; Cheng, X.; Li, B.; Shen, X.; Yan, C.; Huang, J.; Zhang, Q. Highly Stable Lithium Metal Batteries Enabled by Regulating the Solvation of Lithium Ions in Nonaqueous Electrolytes. *Angew. Chem. Int. Ed.* **2018**, *57*, 5301–5305. [CrossRef] [PubMed]
113. Li, P.C.; Chen, L.; Wen, Z.X.; Zhang, D.X.; Zhang, Y.; Zhang, N.; Chen, G.; Liu, X.H. Solvation chemistry of rare earth nitrates in carbonate electrolyte for advanced lithium metal batteries. *Chem. Eng. J.* **2022**, *433*, 134468. [CrossRef]
114. Guo, J.; Wen, Z.Y.; Wu, M.F.; Jin, J.; Liu, Y. Vinylene carbonate-$LiNO_3$: A hybrid additive in carbonic ester electrolytes for SEI modification on Li metal anode. *Electrochem. Commun.* **2015**, *51*, 59–63. [CrossRef]
115. Gu, S.C.; Zhang, S.W.; Han, J.W.; Deng, Y.Q.; Luo, C.; Zhou, G.M.; He, Y.B.; Wei, G.D.; Kang, F.Y.; Lv, W.; et al. Nitrate Additives Coordinated with Crown Ether Stabilize Lithium Metal Anodes in Carbonate Electrolyte. *Adv. Funct. Mater.* **2021**, *31*, 2102128. [CrossRef]
116. Choi, H.; Bae, Y.; Lee, S.M.; Ha, Y.C.; Shin, H.C.; Kim, B.G. A $LiPF_6$-LiFSI Blended-Salt Electrolyte System for Improved Electrochemical Performance of Anode-Free Batteries. *J. Electrochem. Sci. Technol.* **2022**, *13*, 78–89. [CrossRef]
117. Hu, Z.L.; Zhang, S.; Dong, S.M.; Li, W.J.; Li, H.; Cui, G.L.; Chen, L.Q. Poly(ethyl α-cyanoacrylate)-Based Artificial Solid Electrolyte Interphase Layer for Enhanced Interface Stability of Li Metal Anodes. *Chem. Mater.* **2017**, *29*, 4682–4689. [CrossRef]
118. Liu, Q.; Xu, Y.; Wang, J.; Zhao, B.; Li, Z.; Wu, H.B. Sustained-Release Nanocapsules Enable Long-Lasting Stabilization of Li Anode for Practical Li-Metal Batteries. *Nano-Micro Lett.* **2020**, *12*, 176. [CrossRef]
119. Adiraju, V.A.K.; Chae, O.B.; Robinson, J.R.; Lucht, B.L. Highly Soluble Lithium Nitrate-Containing Additive for Carbonate-Based Electrolyte in Lithium Metal Batteries. *ACS Energy Lett.* **2023**, *8*, 2440–2446. [CrossRef]